AD NUMBER

AD876318

LIMITATION CHANGES

TO:

Approved for public release; distribution is unlimited.

FROM:

**Distribution authorized to U.S. Gov't. agencies and their contractors;
Administrative/Operational Use; NOV 1970. Other requests shall be referred to Arnold Engineering Development Center, Arnold AFB, TN.**

AUTHORITY

AEDC ltr 12 Feb 1973

DEVELOPMENT OF A MAGNETIC ANNULAR ARC OPERATING NEAR ATMOSPHERIC PRESSURE

G. W. Garrison, Jr. and R. T. Smith

ARO, Inc.

November 1970

PROPULSION WIND TUNNEL FACILITY

ARNOLD ENGINEERING DEVELOPMENT CENTER

AIR FORCE SYSTEMS COMMAND

ARNOLD AIR FORCE STATION, TENNESSEE

NOTICES

When U. S. Government drawings specifications, or other data are used for any purpose other than a definitely related Government procurement operation, the Government thereby incurs no responsibility nor any obligation whatsoever, and the fact that the Government may have formulated, furnished, or in any way supplied the said drawings, specifications, or other data, is not to be regarded by implication or otherwise, or in any manner licensing the holder or any other person or corporation, or conveying any rights or permission to manufacture, use, or sell any patented invention that may in any way be related thereto.

Qualified users may obtain copies of this report from the Defense Documentation Center.

References to named commercial products in this report are not to be considered in any sense as an endorsement of the product by the United States Air Force or the Government.

DEVELOPMENT OF A MAGNETIC ANNULAR ARC OPERATING NEAR ATMOSPHERIC PRESSURE

G. W. Garrison, Jr. and R. T. Smith
ARO, Inc.

FOREWORD

The work presented herein was sponsored by the Arnold Engineering Development Center (AEDC), Air Force Systems Command (AFSC), Arnold Air Force Station, Tennessee, under Program Element 64719F.

The results of the research presented were obtained by ARO, Inc. (a subsidiary of Sverdrup & Parcel and Associates, Inc.), contract operator of AEDC, AFSC, under Contract F40600-71-C-0002. The research was conducted from July 1, 1969, to June 30, 1970 under ARO Project PW5021, and the manuscript was submitted for publication on August 31, 1970.

Information in this report is embargoed under the Department of State International Traffic in Arms Regulations. This report may be released to foreign governments by departments or agencies of the U. S. Government subject to approval of the Arnold Engineering Development Center (XON), or higher authority within the Department of the Air Force. Private individuals or firms require a Department of State export license.

This technical report has been reviewed and is approved.

David C. Reynolds
Captain, USAF
Research and Development Division
Directorate of Technology

Harry L. Maynard
Colonel, USAF
Director of Technology

ABSTRACT

Two steady-state, high-pressure magnetic annular arc (MAARC) devices are compared experimentally to determine the potential of a MAARC as an ablation facility heat source. Data are presented verifying theory of operation in two modes, one subsonic and the other apparently supersonic. A comparison is made of projected MAARC devices and currently operating conventional high-pressure arc heaters for use as heat sources for high-shear ablation facilities.

CONTENTS

APPENDIXES

I. ILLUSTRATIONS

Figure

NOMENCLATURE

A	Vehicle reference area
B	Magnetic field strength
C_D	Vehicle drag coefficient
$\bar{C}_e$	Electron mean thermal speed
C_p	Specific heat
d_e	Exit diameter of heaters
E_I	Ionization energy
e	Coulombic charge
H_o	Total enthalpy
h	Enthalpy
I	Current
J	Current density
k	Boltzmann's constant
L	Loss to electrodes
ℓ	Anode radius
M	Mach number
M_g	Molecular weight of gas

m	Particle mass
$\dot{m}$	Mass flow rate
n	Particle number density
P_g	Power in the gas
p	Pressure
p_o'	Model stagnation pressure
Q_{es}	Electron-neutral collision cross section
$\dot{q}$	Local heat flux
R	Gas constant
r	Nose radius
r_i	Cathode radius at arc attachment
r_o	Anode radius at arc attachment
T	Temperature
T_o'	Model stagnation temperature
u	Velocity of gas
u_c	Critical speed
V	Voltage
V_o	Total electrode voltage drop
W	Reentry vehicle weight
Z	Gas compressibility factor
α_o	Experimental constant for anode voltage drop
β^*	Defined in Fig. 1
γ_e	Reentry angle
η	Thermal efficiency
ρ	Gas density
ρ_o'	Model stagnation density
σ	Gas electrical conductivity
τ	Time
$\omega_e\tau_e$	Hall coefficient

SUBSCRIPTS

ANODE	Anode
CAT	Cathode
B	Values on the model
e	Electron
i	Ion
o	Stagnation values
r	Radial direction
rec	Recombination
res	Residence
rot	Rotation
s	Neutral species
w	Wall
θ	Azimuthal direction
∞	Free-stream values

SECTION I
INTRODUCTION

The ablation testing of reentry vehicles requires the simulation of a high temperature, high stagnation pressure flow. Various methods have been devised to fulfill the need for such a high-shear ablation facility. The merits of each can be judged by comparing the facility performance with desired test goals. For this purpose, typical reentry trajectories are shown in Fig. 1 (Appendix I) along with the location of maximum stagnation point pressure and laminar stagnation point heat transfer to a hot wall (h_w = 2000 Btu/lb). The range of primary interest is probably between the β^* = 1000 to 2000 lb/ft^2 trajectories (the area shaded in Fig. 1). The test flow should be Mach number 2 or greater so that the pressure distribution over the model nose is a reasonable duplication of that on a reentry vehicle. Model stagnation pressures above 130 atm are required in order to be above the triple point of carbon.

Arc heaters have increased in size and pressure but have fallen short of the desired goals. By nature, all high power, large, arc heaters are inefficient when operated at the high chamber pressures necessary to generate high model stagnation pressures (Ref. 1). NASA (Ref. 2) has combined an arc heater with several radiation lamps to increase the heating rate to the test article. Theoretical and experimental investigations of magnetohydrodynamic (MHD) accelerators combined with large arc heaters have shown that these devices can be expensive and rather inefficient at high pressures. A cold gas flow with heat transfer being provided by a high intensity radiation source (RASTA system at Avco) was developed as an ablation facility, but radiation source problems have made the system difficult to operate. Testing has been done in a rocket exhaust using cyanogen as a fuel to obtain high temperatures. All of these systems have inherent limitations when extended toward the set goals.

One single device combines the action of several of the above devices into one small, compact, highly efficient unit. This is the Magnetic Annular Arc (MAARC). MAARC concepts have been developed for several years as space thrusters [magnetoplasmadynamic (MPD) thrusters] by many researchers. The techniques used in this AEDC program are extensions of those developed at Avco (Ref. 3). The potential of a MAARC can be seen by comparing the expected performance of a 125-MW device with the desired test conditions (Fig. 2). Avco has reached these conditions with pulsed devices (Ref. 4).

SECTION II
THEORETICAL CONSIDERATIONS

The Magnetic Annular Arc (MAARC) combines the action of an arc heater and MHD accelerator but does not suffer from the classical limitations of these devices. The MAARC consists of a center cathode and concentric anode (Fig. 3). A predominantly axial magnetic field is applied by a solenoid-type magnet. The magnetic field and electrical discharge interact to contain and accelerate the plasma which provides a high enthalpy, high stagnation pressure flow. The high magnetic field does not change the ablation characteristics of the model as shown in Appendix III.

Although a complete theory for the operation of the MAARC is not available, the basic processes have been identified. The radial component of the current interacts with the axial component of the magnetic field to exert an azimuthal force causing the plasma to swirl. The energy invested in swirl is converted into directed kinetic energy as the flow expands. This interaction also produces an azimuthal Hall current which can be much larger than the applied current if the Hall coefficient ($\omega_e \tau_e$) is large. Successful operation of the device requires that the Hall coefficient be larger than one. The short-circuited Hall current (1) interacts with the applied magnetic field to increase the voltage and thus increase the power input to the gas for a given arc current, (2) interacts with the radial component of magnetic field to accelerate the flow, and (3) interacts with the axial component of the magnetic field to force the hot plasma away from the walls and thus increase the efficiency of the device. The axial magnetic field also produces a force which increases the pressure on the centerline of the flow.

An additional consequence of the interaction of the magnetic field and electrical current is that the discharge becomes "diffuse" at higher magnetic field strengths. At zero or low magnetic field strengths, the discharge appears as a constricted column or "spoke." As the magnetic field strength is increased, the rotational frequency of the spoke increases until its rotational period is less than the characteristic recombination time and gas residence time in the discharge. The spoke then disappears, and the discharge appears to fill the annular space between the cathode and anode; i. e., the discharge is diffuse. The diffuse discharge results in low electrode erosion and uniform heating and acceleration.

The processes enumerated do not explain fully the operation of the MAARC. Different modes of operation have been observed during a

given firing without any change in the controllable parameters. The phenomena causing the change in operating modes have not been identified.

The electrons are the current-carrying species within the discharge and are the predominant contributors to the heat transfer at the anode. However, the current-carrying processes at the cathode surface are not well defined, and it is not understood how the cathode can support such apparently high current densities without significant erosion. Some plausible explanations have been posed (Ref. 5), but experimental verification is difficult.

It is apparent that a complete theory for the operation of the MAARC may be difficult, if not impossible, to formulate although many investigators have reported data from such devices (Refs. 6 through 17). Some insight into the various processes occurring in the discharge have been obtained using a quasi-one-dimensional approximation (Refs. 18 and 19). However, these do not account for radial distributions nor for the energy transfer at the electrodes. An investigation has been initiated at AEDC which considers the flow to be axisymmetric and requires specification of the boundary conditions on the electrodes. The mathematical model considers the flow of a multispecies, two-temperature plasma through the interaction region of the MAARC. The describing equations have been programmed, and a concerted effort is being made to obtain solutions which will provide insight into the basic phenomena occurring in the device and also predict the overall characteristics of the device.

Although a complete theory for the MAARC does not exist at present, some indication of the expected performance can be obtained using approximate expressions and certain empirical relations obtained from experiment. It is observed from experiments (see Section IV) that the heat loss to the anode ($\dot{Q}$) varies linearly with the total current I; that is,

$$\dot{Q} = \alpha_o V_o I \tag{1}$$

where $\alpha_o V_o$ (Ref. 3) is the anode voltage drop and α_o is a constant ($0.5 < \alpha_o < 1$). By assuming that the effective current-carrying area of the anode is $(2\pi\ell)\ell$, where ℓ is the anode radius, the heat transfer to the anode is

$$\dot{q} = \frac{\alpha_o V_o I}{2\pi\ell^2} \tag{2}$$

It is also observed experimentally that the voltage of the device varies linearly with the applied magnetic field. The voltage drop has

been related to the critical ionization speed (Ref. 20) with the resulting expression for the MAARC geometry (Ref. 3)

$$V = V_o + u_c B\ell' \tag{3}$$

where V_o is the voltage drop near the electrodes and u_c is the critical speed given by

$$u_c = \sqrt{\frac{2E_I}{m_i}}$$

The quantity E_I/m_i is the ratio of the ionization energy to the mass of the ion, and u_c has a value of 1.6×10^4 m/sec for nitrogen and air. The quantity V_o is determined empirically and has a value of 30 v for nitrogen.

It is now assumed that the mass flow rate ($\dot{m}$), total enthalpy, (H_o), and model stagnation pressure (p_o') can be expressed by the following simple relations

$$\dot{m} = \rho_\infty u_\infty (\pi \ell^2) \tag{4}$$

$$H_o = \frac{u_\infty^2}{2} = \frac{P_g}{\dot{m}} = \frac{I u_c B \ell}{\dot{m}} \tag{5}$$

$$p_o' = \rho_\infty u_\infty^2 \tag{6}$$

where ρ is the gas density, u is the velocity and P_g is the power in the gas. By using these expressions and the limiting factors observed from experiments, an operating envelope can be defined for the MAARC.

The first limit to be considered concerns the maximum allowable heat transfer to the anode. Equation (2) and Eqs. (4) through (6) may be used to obtain an inequality for the heat transfer limit line for the MAARC. It can be written as

$$H_o \leq \frac{2^{7/3}}{\pi^{2/3}} \left(\frac{u_c B q_{max}}{\alpha_o V_o} \right)^{4/3} \frac{P_g^{2/3}}{p_o'^2} \tag{7}$$

where $\dot{q}_{max}$ is the maximum allowable heat transfer to the anode. Present technology limits the heat load that can be transferred by back-side water cooling to approximately 10 kw/cm^2.

Successful operation of the MAARC requires a large Hall current and, hence, a large Hall coefficient. Then, the second requirement for

the MAARC operating envelope is that the Hall coefficient be larger than some minimum value. This can be expressed as

$$\omega_e \tau_e = \left(\frac{eB}{m_e}\right) \frac{1}{n_s Q_{es} \bar{C}_e} > (\omega_e \tau_e)_{min} \tag{8}$$

where e/m_e is the electron charge-mass ratio, n_s is the particle number density of neutral species, Q_{es} is the collision cross section, and $\bar{C}_e$ is the electron mean thermal speed ($\sqrt{8kT_e/\pi m_e}$), where T_e is the electron temperature. Since $n_s = \rho/m_s$ and by using $Q_{es} = 10^{-19}$ m^2 and $T_e = 8000°K$, Eq. (8) can be written as

$$\frac{BM_g}{\rho_\infty} \frac{1}{290} > (\omega_e \tau_e)_{min} \tag{9}$$

where M_g is the molecular weight of the gas. Combining Eq. (9) with Eq. (5) and Eq. (6) gives

$$H_o \geq \frac{190}{2} \frac{p_o'}{BM_g} \quad (\omega_e \tau_e)_{min} \tag{10}$$

The equations for the limiting curves can be written for fully dissociated nitrogen as

$$H_o \leq 1.97 \times 10^5 \frac{(P_g)^{2/3} (B)^{4/3}}{(p_o')^2} \quad \text{Heat Transfer Limit Line} \tag{11}$$

$$H_o \geq 0.592 \times 10^3 \frac{p_o'}{B} \quad (\omega_e \tau_e) \text{ Limit Line} \tag{12}$$

$$\ell \geq 2.185 \times 10^{-2} \sqrt{I} \tag{13}$$

$$I = 4.35 \times 10^3 \left(\frac{P_g}{B}\right)^{2/3} \tag{14}$$

$$V = 230 (P_g)^{1/3} (B)^{2/3} \tag{15}$$

The value of $(\omega_e \tau_e)_{min}$ is assumed to be two. The units of Eqs. (11) through (15) are: H_o, Btu/lbm; P_g, megawatts; B, tesla; p_o', atm; ℓ, cm; I, amp; and V, volts.

The operating envelope for a MAARC utilizing a 25-tesla magnet with 125 MW in the gas was shown previously in Fig. 2. This device would provide the enthalpy and stagnation pressures necessary for ablation testing of ballistic reentry vehicles in the region of primary interest. The operating envelope for a 15-MW device using a 10-tesla

magnet is also shown. This device would provide flow of 10,000 Btu/lbm at a model stagnation pressure of 50 atm.

SECTION III
TEST DESCRIPTION

3.1 TEST INSTALLATION

The test installation (Fig. 4) consisted of the previously tested (Ref. 21) HP-2M MAARC or the AEDC-designed Hera M1 MAARC, free-jet test area, probe injection system, exhaust duct, and air ejector. The MAARC and magnet were the only highly cooled components in the circuit. The probe injection system used uncooled graphite pressure probes and ablation models for macroscopic determination of the flow parameters. The single probe was injected laterally into the flow and could be stopped at any predetermined position or allowed to pass through the flow. Axial probe positioning was done manually before the heater run was started. The probe could be aligned vertically by manual adjustment of the injection platform. An air ejector was used to increase the pressure ratio to ensure supersonic flow in the nozzle before firing.

3.2 MAGNETIC FIELD COIL

The magnetic field coil was obtained from the Air Force Flight Dynamics Laboratory along with a MAARC herein designated as the HP-2M. The coil consisted of 24 discs in electrical series with adjacent pairs in hydraulic parallel and is described in detail in Ref. 21. A photograph of the coil is shown in Fig. 5. The coil was operated at electrical currents up to 3150 amp resulting in coolant temperature rises of 100°F. Field strengths up to 2.6 tesla were obtained at the center point of the coil. Figure 6 shows the axial and radial distribution of the field as measured with a gaussmeter.

3.3 POWER SUPPLIES

An existing 1-MW power supply originally used to drive an iron-core field magnet was modified to provide power for the MAARC. Saturable core reactors were used to control the silicon diode rectifiers so that current up to 2000 amp at voltage up to 500 v was available. After some difficulty with current surges during arc breakdown, a system was derived which controlled within acceptable limits.

The power supply used to drive the 2.5-tesla magnetic field coil was designed to deliver 875 kw at either 125 or 250 v. Saturable core reactors were used to control the silicon diode rectifiers so that current could be controlled from 20 percent to full range.

3.4 GAS SUPPLY SYSTEM

Nitrogen was gasified and pumped from a central liquid-nitrogen storage point at AEDC to the test area. It was supplied to the test site at 2100 psi and then reduced to the pressure needed for proper control of the MAARC through a small electrically operated pressure regulating valve. The flow was measured using an instrumented choked convergent-divergent nozzle designed using standards accepted at AEDC (Ref. 22). The mass flow measurement system was carefully calibrated and checked to ensure the accuracy of the mass flow.

3.5 WATER SYSTEM

The HP-2M MAARC was cooled using the low-pressure raw water system. Raw water is pumped from a large lake to a storage reservoir at AEDC. It is pumped out of the reservoir through a 100-psi pump where calgonites are added to discourage algae attaching to lines and experimental apparatus. The water is filtered before entering the test building. Inside the test building, the water pressure is boosted to 300 to 400 psi at flow rates up to 8000 gpm to the MAARC test area. The water was filtered a second time before entering the experimental equipment using 100- and 15-micron filters in series. The HP-2M used only 70 gpm, thereby resulting in a considerable amount of water to be bypassed.

Closed-loop demineralized water systems were used to cool the Hera-M1 MAARC and the 2.5-tesla coil. The Hera was cooled by a pump delivering 60 gpm at 600 psi through a pressure-controlled manifold. The coil used a pump delivering 1000 gpm at 3750 psi through a control valve and bypass system to deliver 70 gpm at 1200 psi to the coil. The pump inlet pressure had to be maintained at 400-psi minimum pressure. The water was circulated through a water-to-water heat exchanger which uses raw lake water as its heat sink.

Insulated Nylon hoses were used to connect the MAARC and coil to the water manifolds. Water temperature sensors and pressure transducers were installed in the manifold taps to monitor temperature rises and water pressure during the run.

3.6 INSTRUMENTATION AND DATA REDUCTION

The data acquisition system used for this investigation is a modified 100-channel Beckman 210 high-speed data system which is used to digitize signals in the range of 0 to 80 mv. A 100-channel commutator is used to sequentially gate the outputs of 100 highly stable d-c preamplifiers into a single analog-to-digital converter. The digital information is usually recorded on magnetic tape for later entry into the computer as an off-line operation.

The heart of the digital data processing system is the PWT Computer System, consisting of two modified Raytheon 520 computers coupled with several types of memory and peripheral devices. Computed data are tabulated on 300-line/min printers located in the computer room. In addition, a 14-channel FM tape system and oscillograph are used to observe dynamic data.

Standard facility measurements were: MAARC voltage and current, magnet voltage and current, gas flow rates, gas supply pressures, MAARC pressures, coolant flow rates and temperatures, and various other critical parameters as required.

The d-c power to the MAARC was determined by continuously monitoring the operating voltage and current. The mass flow rate of the gas was measured with a choked orifice located upstream of the MAARC. The gas pressure (MAARC pressure) was measured several cathode diameters upstream of the discharge to better understand the gas dynamics of the flow. The water flow rates and the temperature rise of the cooling water to the electrodes were used to determine the energy loss in the device from which the heater efficiency and heat balance enthalpy were calculated. Combining the energy balance with the airflow rate gives the bulk or heat balance enthalpy:

$$H_o = \left[V I - (\dot{m} C_p \Delta T)_{H_2O}\right] / \dot{m}_{gas} + \left[C_p T_{inlet}\right]_{gas}$$

In all, a total of twenty-six parameters were measured, and ten calculated parameters were programmed in the data reduction.

A 16-mm Hycam® high-speed camera which had a framing rate up to 11,000 frames/sec with a shutter speed of 2 μsec was used to determine the form of the arc column; i. e., filament or disk, as a function of axial magnetic field strength. A second 16-mm camera operated at 64 frames/sec was used to obtain good quality flow photographs for detailed analysis.

3.7 TEST PROCEDURE

After determining that the MAARC was properly fused between the cathode and anode, all water and gas systems were brought to the ready status. The air ejector, when used, was charged, and the test cell pressure was reduced to about 1.5 psia. The master power breaker was closed, vaporizing the fuse to start the discharge. Under normal operating conditions of this series of tests, the arc was initiated and stabilized within a few msec. All instrumentation reached steady state in about 5 sec. Operation could be maintained for minutes without significant changes in operating parameters except as noted later with the Hera. Test conditions were changed during operation by varying the air pressure, arc current, and/or magnetic field. The heater run was terminated by opening the master power breaker which shuts off the electrical power. The gas isolation valve was closed and the prefire procedure was reversed.

All water systems were interlocked so that failure of any component to meet set requirements shut off all direct-current power to the device and coil.

SECTION IV
HP-2M MAARC

The HP-2M MAARC, a modified version of a device designed for low-pressure operation (Ref. 21), was operated on nitrogen exhausting to atmosphere to determine performance trends and to obtain a diffuse discharge. This MAARC consisted of a constant-area coaxial copper anode 1.40 in. (3.40 cm) in diameter and a cathode 1.00 in. (2.54 cm) in diameter. The cathode tip was hemispherical, and both copper and thoriated tungsten were used. A photograph of the disassembled HP-2M is shown in Fig. 7. The water-cooled anode-cathode assembly could be positioned with respect to the magnetic field coil by clamps, and the length of the anode allows testing at positions from the center to the exit of the field coil. The cathode could be moved freely into any position with respect to the anode. The anode tip was threaded so that the anode tip diameter could be changed to determine its effect.

Considerable data were taken with this device operating in a subsonic mode exhausting to atmospheric back pressure. The basic data curves of enthalpy, voltage, efficiency, and electrode losses plotted versus magnetic field, current, and gas flow rate are presented in Figs. 8, 9, and 10. The more pertinent data are discussed in detail.

Figure 8 shows the variation of enthalpy, voltage, and efficiency with increasing magnetic field for both the copper and tungsten cathodes. Operation with a tungsten cathode invariably gave a higher voltage and efficiency, thus a higher enthalpy. The cathode heat loss using tungsten was approximately one-half of that for copper. This may be attributed to the thermal emission of the tungsten tending to cool the cathode. The overall efficiency of the device increased with magnetic field because of the decrease of the fraction of the power loss to the cathode and anode. The voltage, using either material, increased linearly with increasing magnetic field, agreeing with earlier experimental results (Refs. 3 and 21).

The MAARC has a drooping V-I characteristic except at high current and high magnetic fields where the slope becomes positive. This voltage characteristic, as well as the variation of enthalpy and efficiency with current, is shown in Fig. 9. The anode power loss generally increased linearly with increasing current, but the cathode loss was usually independent of current. The overall efficiency of the device decreased slightly and then increased as the current increased. The enthalpy changed rapidly with increasing current, and the maximum enthalpy measured (based on a heat balance) during the series of tests was 18,000 Btu/lbm. This is not a MAARC limit but a system limit.

As the mass flow increased and if the voltage remained constant, the fraction of power loss to the cathode was constant or increased slightly as seen in Figs. 10a, b, and c. Figures 10d and e show that, if the voltage increased with increasing mass flow rate, the fraction of power loss to the cathode decreased. The anode loss decreased with increasing mass flow; thus the overall efficiency of the device increased in both cases.

Figure 11 shows the variation of the overall efficiency of the device with total power and includes data from other facilities. These earlier data indicate that the efficiency increased with power, achieving an efficiency above 95 percent at the 100-MW level. This trend was verified in the present device using both copper and tungsten cathodes. An efficiency of 70 percent was obtained at 0.4 MW using the copper cathode, and 85-percent efficiency was obtained at 0.2 MW using the tungsten cathode.

Three sets of consecutive frames taken from the high-speed films of the discharge are shown in Fig. 12. Each set is typical of the discharge at the operating conditions specified. The photographs in Fig. 12a were taken at a field strength of B = 0.265 tesla, current I = 760 amp, and a mass flow of $\dot{m}$ = 0.014 lbm/sec. At this condition, the

discharge consisted of a concentrated current path, or "spoke", and is typical of the discharge in conventional arc heaters. The "spoke" rotated at a measured frequency of 3180 Hertz. By assuming that the gas rotates as a solid body, an expression for the rotational frequency can be derived as $\omega = \frac{IB}{\dot{m}2\pi}\left(\frac{r_o^2 - r_i^2}{r_o^2 + r_i^2}\right)$ where r_i and r_o are the inner and outer electrode radii, respectively. This yields a frequency of 1509 Hz for this device. If the discharge occurs at the cathode tip, then $r_i \sim 0$, and a frequency of 5060 Hz is obtained. These values bracket the measured frequency indicating that the discharge originated somewhere between the tip and the outer surface of the cathode. Inspection of the cathode after operation confirms these observations.

In order for the discharge to completely fill the annulus between cathode and anode (i. e., become diffuse), the time for the spoke to make one rotation ($\tau_{rot} = 1/\omega$) must be much less than the residence time (τ_{res}) and/or the characteristic time for recombination (τ_{rec}) (Ref. 23). For the conditions of this experiment, $\tau_{rec} \approx 1,000\,\mu$sec, $\tau_{res} \approx 200\,\mu$sec; for Fig. 12a, $\tau_{rot} \approx 400\,\mu$sec. The criteria for a diffuse discharge were not met.

The visible current path appeared to fluctuate between a spoke and diffuse discharge for the conditions in Fig. 12b. Although the time to make one revolution was 70 μsec, the current was apparently not high enough to sustain a steady diffuse discharge.

The calculated rotational time for the conditions in Fig. 12c is 30 μsec, which is less than the recombination and the residence time, and the necessary conditions for a diffuse discharge are present. Also, a spoke rotating at 500, 000 Hz ($\tau_{rot} \approx 2\,\mu$sec) can be photographed by the camera, but no confirmed current path was detected. Hence, the discharge shown in Fig. 12c is considered diffuse.

Although the magnetic fields utilized were relatively low, the performance obtained with the HP-2M indicated that successful operation at atmospheric pressure is possible. The basic criteria are fulfilled for the operation of a MAARC providing supersonic flow with high stagnation pressure and high enthalpy. A MAARC of improved design was fabricated and is discussed in the next section.

SECTION V
HERA MAARC

The Hera MAARC was designed for operation at 1 MW using the available power supplies and magnet. The anode radius was chosen as the minimum which satisfied the anode heat transfer requirement (Section II). For operation at 1 MW, a magnetic field of approximately 3 tesla is required to satisfy the minimum Hall coefficient requirement. It was realized that the available axial magnetic field (2.5 tesla) would be marginal at best and that the device should be operated at a combination of axial and radial field rather than full axial field. Operating away from the center of the magnet considerably reduces the effective field strength and power at which the Hera could be operated. The power supply presented an additional limit since the maximum available voltage was 500 v and any external ballast added for stability reduced the available voltage.

The Hera MAARC (Fig. 13) consisted of a 0.787-in. (2.00 cm) diam anode and a nominal 0.400-in. (1.02 cm) cathode. The anode was water-cooled copper, and the cathode was a tungsten-copper alloy. The device was mounted on an adjustable stand so that it could be positioned in the magnetic field at optimum locations. The cathode was electrically insulated and supported by a long finned support. The cathode was contoured to give a minimum area between it and the anode with an expansion to a nominal cold nitrogen flow Mach number of 1.7 where the discharge should occur.

Considerable difficulty was encountered with a pliant cathode during starting transients. Electromagnetic forces were large enough to move the cathode sideways causing the electrical insulator to collapse, resulting in cathode failure due to impact on the anode. A rigid insulator was installed between the cathode and anode, and the problem was eliminated.

Most of the runs were subonic because of a combination of lower than required magnetic field, arc attachment at cathode shoulder rather than at the tip, and insufficient power to produce a high enthalpy at the MAARC pressure necessary to expand to the design Mach number. If the MAARC pressure was raised, then the gas flow rate increased resulting in a lower than desired enthalpy. This lower enthalpy decreased the Hall coefficient to a point where the device could not accelerate or magnetically pinch. In addition, increasing the gas flow rate at fixed current and magnetic field caused the diffuse discharge to become "spoked."

Occasionally, the flow was intermittently subsonic and pinched; remaining in each mode for several seconds. Figure 14 shows photographs of the discharge and the resulting gas flow. The side photographs were taken at 10 anode diameters downstream of the discharge. Note the difference in arc location and appearance when the effluent changed from the typically plumed subsonic flow to the pinched apparently supersonic jet. Cathode and anode heat transfer decreased by a factor of two when the device operated in the pinched mode. The decrease in anode heat transfer can be attributed to the jet being constricted away from the anode wall.

Figure 15 is a graphical representation of various MAARC parameters measured as the device changed modes. Note that the MAARC pressure was exactly the same when the device was operating pinched as when no discharge was present in the flow (the device was choked during cold-flow operation). This is convincing evidence of the presence of supersonic flow entering the discharge, and the exit flow was apparently supersonic based on the pictorial evidence in Fig. 14. The MAARC pressure rose significantly when heat was added to the subsonic flow mode. The efficiency and enthalpy make abrupt changes when the device changed to the pinched mode resulting in a very high efficiency (92 percent) and a doubling of the flow enthalpy. Table I (Appendix II) presents a listing of measured and calculated Hera M1 parameters when the device was operating in both modes. Note, in particular, that the calculated model stagnation pressure increased when the flow was pinched.

Figure 16 summarizes the results of both MAARC devices showing improvement due to supersonic operation. The power supply limit mentioned earlier can be seen by studying Fig. 17. The MAARC voltage was limited because the voltage drop across the resistor bank in series with the MAARC reduced the available power supply voltage.

Although other investigators have repeatedly commented on the anode heat load as the major problem with these devices, experience with the present investigation indicates that the anode will last indefinitely at design conditions. The cathode erosion was severe when the MAARC was subsonic and rather insignificant when operating pinched. A comparison of the cathode heat load for the various modes of operation gives some indication of the cause for the high erosion. When the Hera M1 MAARC operated in the subsonic mode, the heat lost to the cathode (center electrode) was 7 to 8 percent of the total power; when operated in the pinched mode, the loss was 2 to 3 percent of the total power. The device was also operated with reverse polarity, and the heat loss to the center electrode was found to be 4 to 5 percent of the total power. No

pinching was observed when operating with reverse polarity. The higher heat load on the center electrode when it serves as a cathode, as opposed to anode, indicates that the ion current must be high near the electrode when operating in the subsonic mode (Ref. 24). The large ion current would then partially explain the high erosion rate observed in the subsonic mode. The lower heat transfer to the cathode measured when operating in the pinched mode indicates a smaller ion current and, hence, less erosion. Since the magnetic field was lower than desired, the intermittent subsonic-pinched operation caused many cathode failures. The use of a higher strength magnet should eliminate cathode failures caused by the higher heat loads when operating subsonically.

Figure 18 shows a comparison of data taken on these two high-pressure devices and a comparison of the anode heat transfer data with thruster and high-pressure pulsed devices. Figure 19 shows a similar comparison of thermal efficiency of present and past devices.

SECTION VI
DISCUSSION AND CONCLUSIONS

In conclusion, it can be stated that there does not appear to be any fundamental physical effect that prevents the MAARC technology from being extended to produce a high-shear ablation test facility with 10,000 Btu/lb stagnation enthalpy and model stagnation pressures approaching 200 atm. The experimental program presented here (although not complete) points the way to high-pressure, high-power MAARC designs. A diffuse arc has been obtained and photographed, and voltages nearly independent of current and directly proportional to the magnetic field were also measured. A device has been operated in a subsonic and apparently supersonic mode with increases in stagnation pressure across the device of 4.25 to 1. A larger magnet will allow data to be obtained at higher powers and pressures.

Table II shows a comparison of data from various arcs with the projected performance of MAARC devices. The parameter $H_o\sqrt{p_o}$ is a stagnation point heat transfer parameter that theoretically puts all arc devices on the same comparison scale. The fallacy with the "standard" comparison is that it does not take into account the test flow size. If size is not considered, a small 50-kw arc heater may show better heat transfer capability than the larger facilities, but the flow size is too small to test actual ablation samples. The parameter $H_o\sqrt{p_o'}\, d_e^2$ allows the total heat transfer capability of various facilities to be

compared. It becomes apparent that a MAARC can produce a very hostile environment and a large diameter flow without the convection and radiation losses associated with a conventional arc heater (i. e., low thermal efficiency). Note that the efficiency measured compares favorably with previous data and shows the trend toward 100-percent efficiency operation as power is increased.

This trend can be explained by writing the expression for efficiency in the form

$$\eta = \frac{IV - \text{Losses}}{IV}$$

$$\eta = 1 - \frac{\alpha_o V_o}{V} - \frac{L_{CAT}}{IV}$$

Since the loss due to the voltage drop at the anode ($\alpha_o V_o$) is constant and L_{CAT} is small, increasing the power (voltage) leads to greater efficiency. Also, the power of the device increases directly with size as a normal arc heater does and also increases with magnetic field. Therefore, it can clearly be seen that a small device can operate at enormous powers if a magnetic field of sufficient strength is available.

REFERENCES

1. Smith, R. T. and Folck, J. L. "Operating Characteristics of a Multi-Megawatt Arc Heater Used with the Air Force Flight Dynamics Laboratory 50-Megawatt Facility." AFFDL-TR-69-6, April 1969.

2. Gowan, F. E. and Nichels, F. H. "The Ames Combined Heating Facility." AIAA Paper 69-342, May 1969.

3. Patrick, R. M. and Schneiderman, A. M. "Performance Characteristics of a Magnetic Annular Arc." AIAA Journal, Vol. 4, No. 2, February 1966, pp. 283-290.

4. Schneiderman, A. M., Pugh, E. R., and Patrick, R. M. "Magnetic Annular Arc-Driven Shock Tube." Physics of Fluids, Vol. 11, No. 2, February 1968, pp. 278-294.

5. Cann, G. L. "Study of Electrode Attachment Regions in High-Current Gaseous Discharges." AEDC-TDR-64-107 (AD603342), August 1964.

6. Mallaris, A. C. "Phenomena in the Cathode Region of an MPD Accelerator." AIAA Paper No. 67-47, January 1967.

7. Rosciszewski, Jan. "Acceleration Process in the Hall Current Device." Physics of Fluids, Vol. 10, May 1967, pp. 1095-1099.

8. Clark, K. E. and John, R. G. "The Magnetoplasmadynamic Arcjet." Astronautical Acta., Vol. 13, No. 4, 1967.

9. Cann, G. L. and Marlotte, G. L. "Hall Current Plasma Accelerator." AIAA Journal, Vol. 2, July 1964, pp. 1234-1241.

10. Schneiderman, A. M. and Patrick, R. M. "Axial Current Distribution in the Exhaust of the Magnetic Annular Arc." AIAA Journal, Vol. 5, No. 2, February 1967, pp. 249-253.

11. Hassan, H. A., Hess, R. V., and Grossman, W. "Study of Coaxial Hall Current Accelerators at Moderate Pressures." NASA TN D-3286, October 1966.

12. Nerheim, N. M. and Kelly, A. J. "A Critical Review of the State-of-the-Art of the MPD Thruster." AIAA Paper No. 67-688, AIAA Electric Propulsion and Plasmadynamics Conference, September 1967.

13. Schneiderman, A. M. and Patrick, R. M. "Optimization of the Thermal Efficiency of the Magnetic Annular Arc." Avco Everett Research Report RR-241, March 1966.

14. Powers, W. E. and Patrick, R. M. "A Magnetic Annular Arc." Avco Everett Research Laboratory, RR-129, May 1962.

15. Powers, E. E. "Measurements of the Current Density Distribution in the Exhaust of an MPD Arcjet." AIAA Journal, Vol. 5, No. 3, March 1967.

16. Patrick, R. M. and Pugh, E. R. "Laboratory Simulation of Solar Wind Phenomena." Proceedings of Sixth Gas Dynamics Symposium, August 1965, and AIAA Paper No. 65-625.

17. Van Camp, W. M., et al. "Study of Arc-Jet Propulsion Devices." NASA CR-5491 or McDonnell Report E368, March 1966.

18. Seals, R. K., Jr. and Hassan, H. A. "Analyzing MPD Arcs with Nonequilibrium Ionization." AIAA Paper No. 68-87. Also AIAA Journal, December 1968.

19. Workman, J. B. "Arc Structure in a Magnetic Annular Discharge." AIAA Journal, Vol. 7, March 1969, pp. 512-519.

20. Alfrien, H. "Collisions between a Nonionized Gas and a Magnetized Plasma." Review of Modern Physics, Vol. 32, 1960.

21. Richter, R., Lenn, P. O., and Buhler, R. D. "Axisymmetric Hall-Arc Jet Wind Tunnel Driver Study." AFFDL-TR-66-213, April 1967.

22. Grace, H. P. and Tapple, C. E. "Discharge Coefficients of Small-Diameter Orifices and Flow Nozzles." Transactions of ASME, Vol. 73, 1951, pp. 639-647.

23. John R. R., et al. "Theoretical and Experimental Investigation of Arc Plasma-Generation Technology Part II, Vol. 2." ASD-TDR-62-729, September 1963.

24. Lenn, P. O., Bodoia, J. R., Ward, D. L., Hamilton, G. L., and Demetriades, S. T. "Three-Fluid Nonequilibrium Plasma Accelerators, Part II." AIAA Electric Propulsion Conference, March 1963, and AIAA Paper No. 63-047.

25. Pugh, E. R., Patrick, R. M., and Schneiderman, A. M. "Properties of Collisionless Plasmas." AFOSR-70-00388 TR, January 1970.

26. Porter, R. W. and Cambel, A. B. "Hall Effect in Flight Magnetogasdynamics." AIAA Journal, Vol. 5, No. 12, December 1967.

APPENDIXES

I. ILLUSTRATIONS
II. TABLES
III. EFFECT OF B-FIELD ON ABLATION TESTING

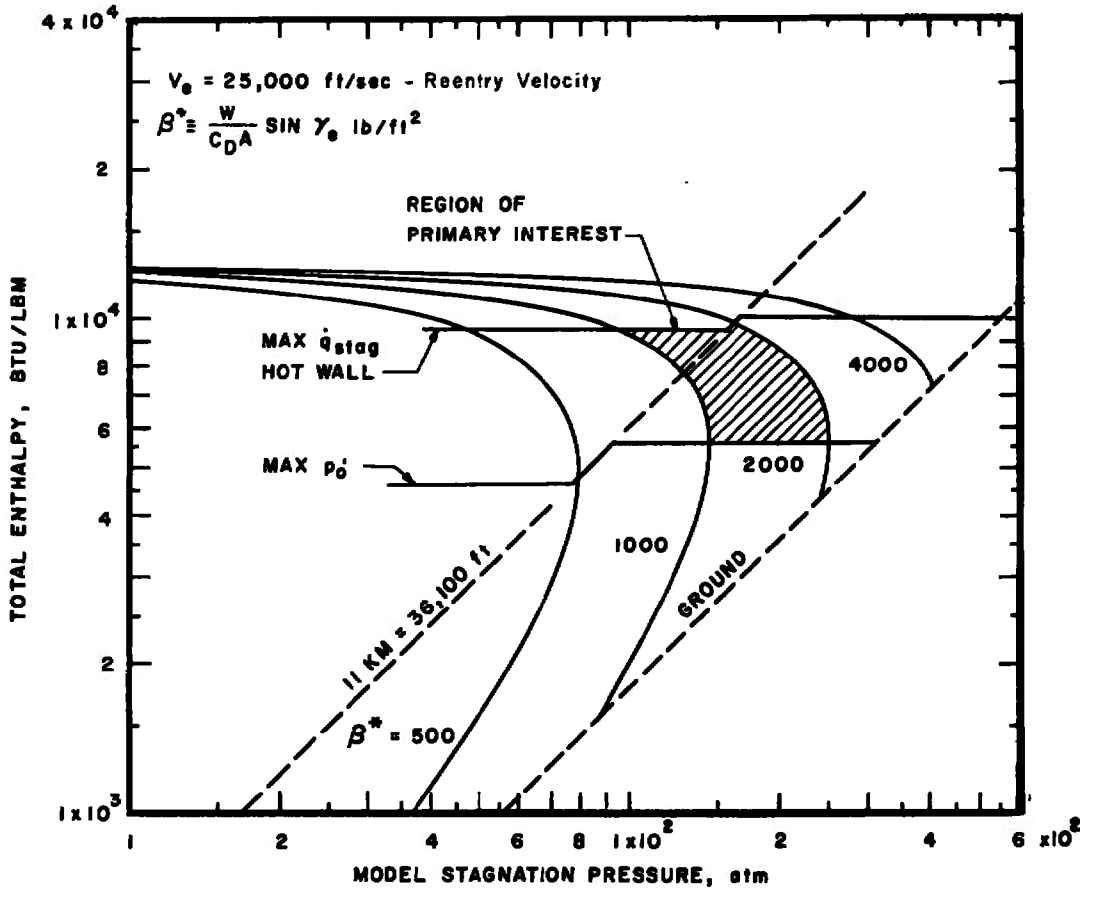

Fig. 1 Ballistic Reentry Trajectories

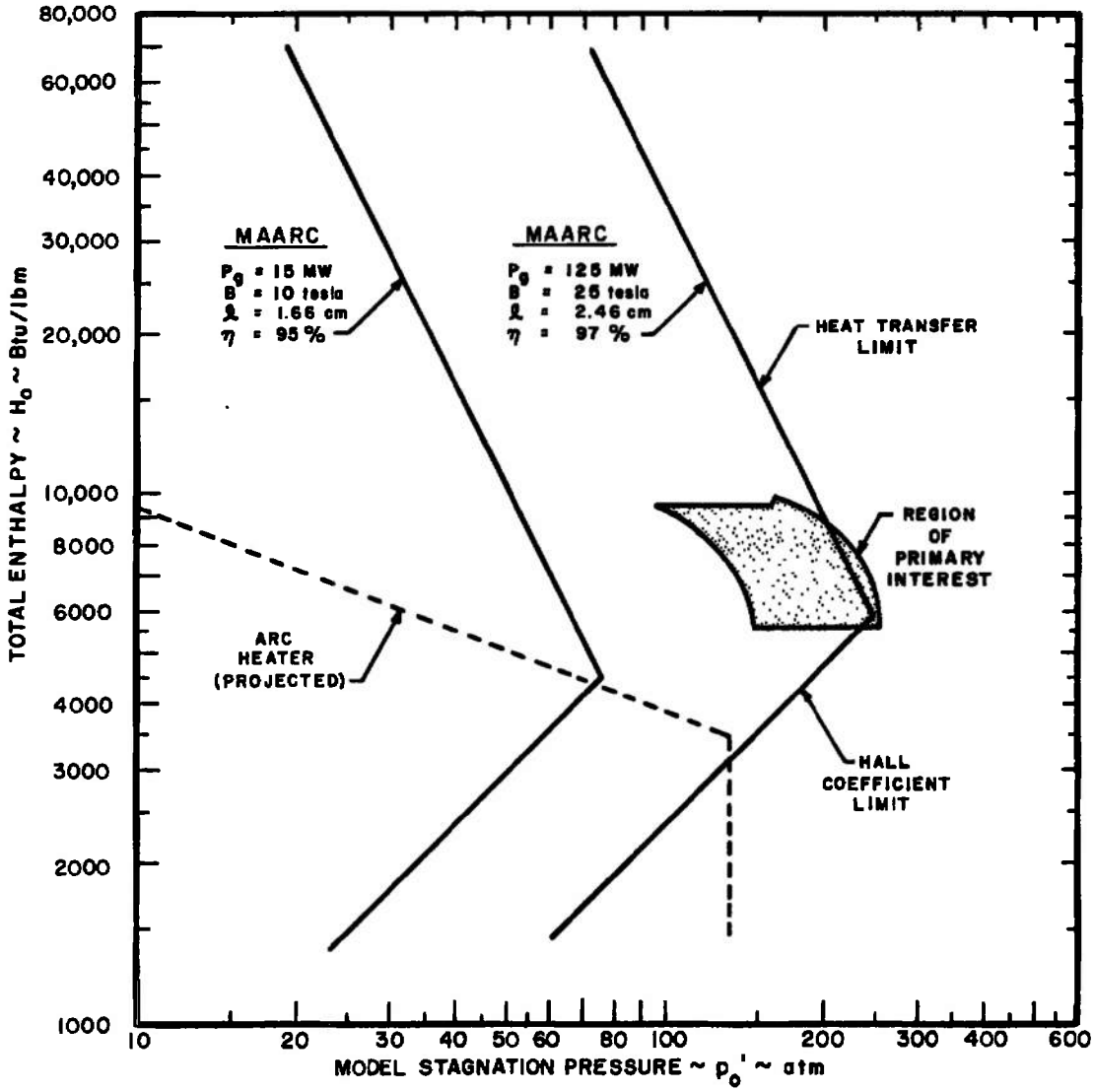

Fig. 2 Comparison of Projected Performance Limits of the MAARC and of Arc Heaters

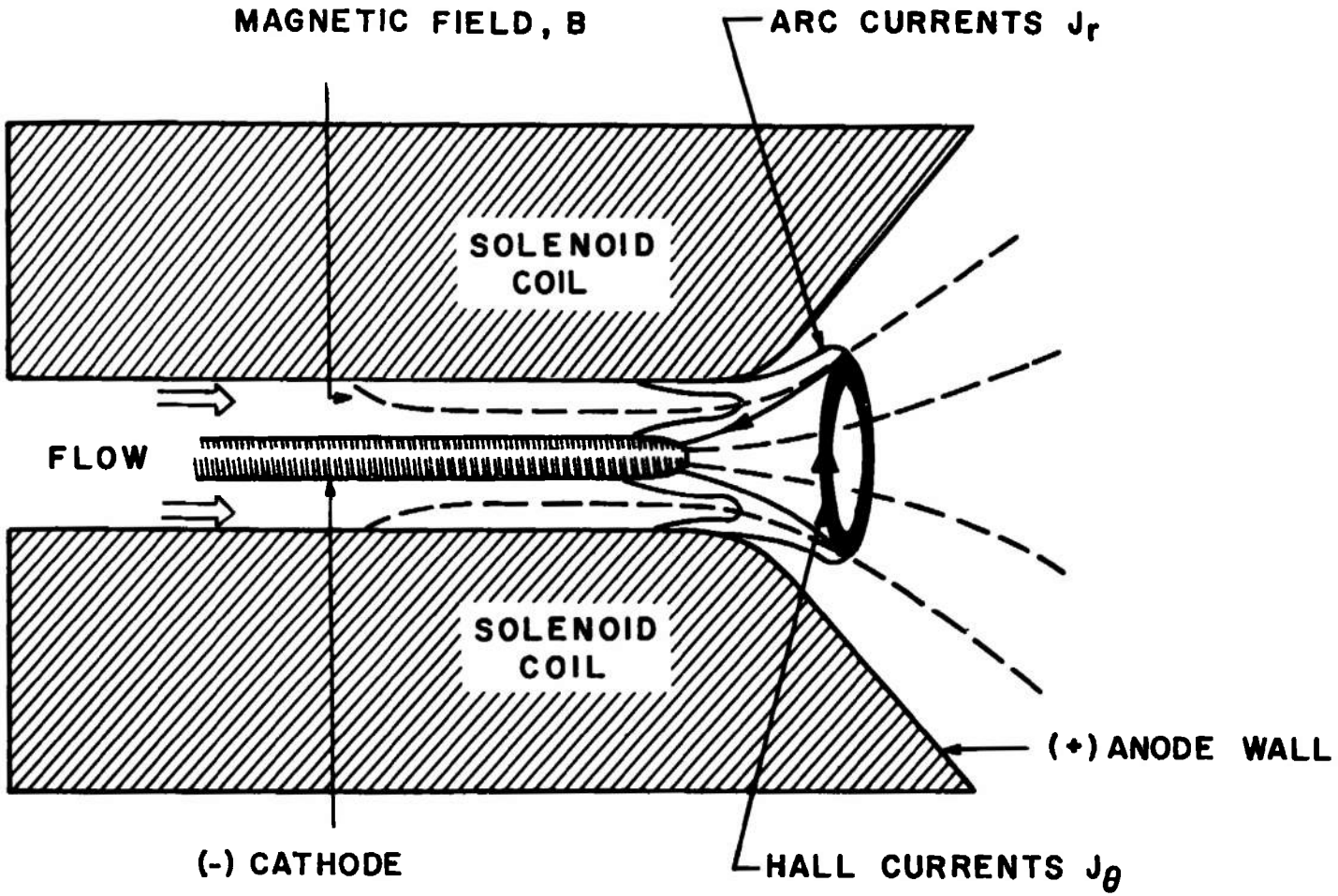

Fig. 3 Schematic of the MAARC

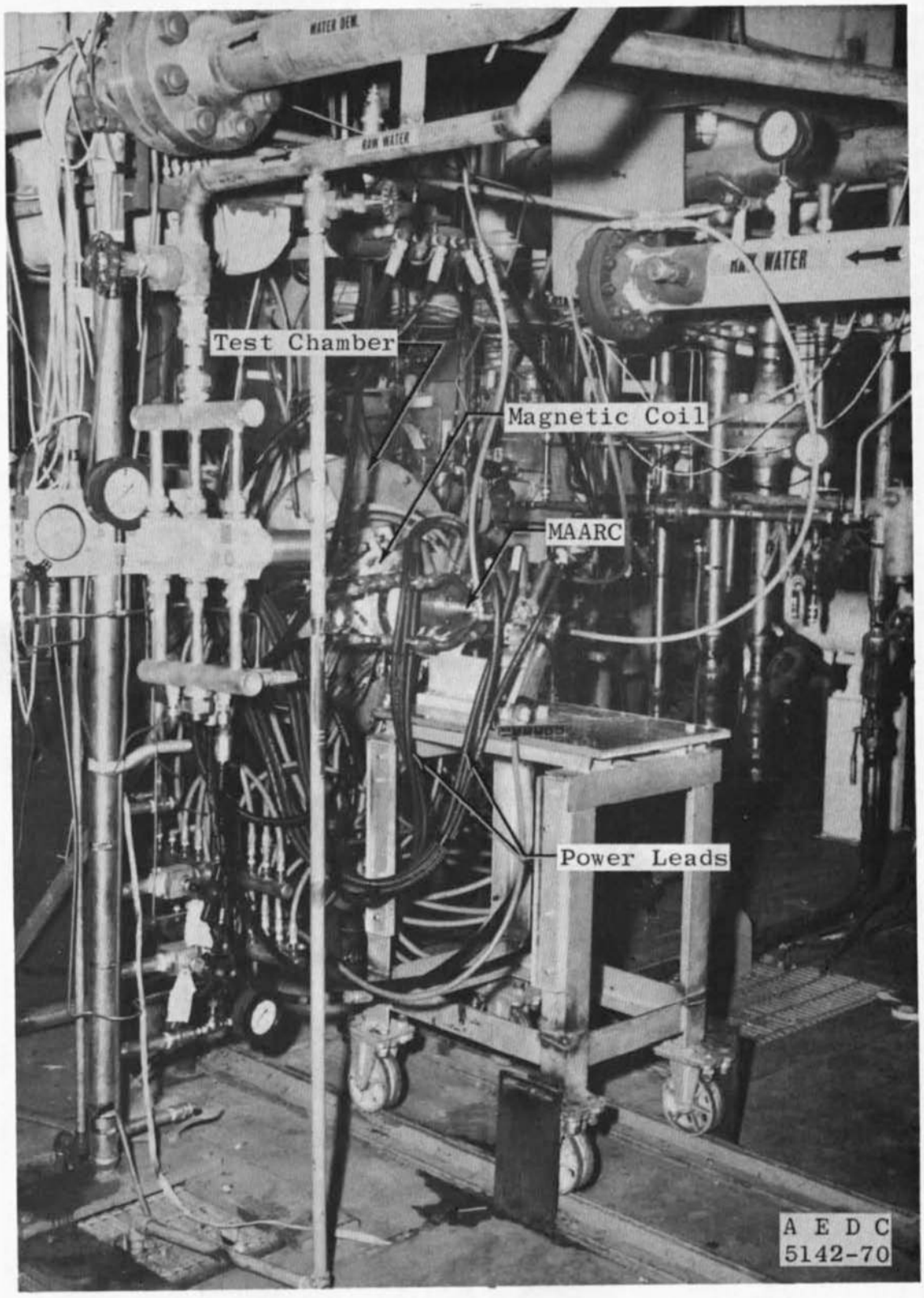

Fig. 4 Photograph of Test Installation

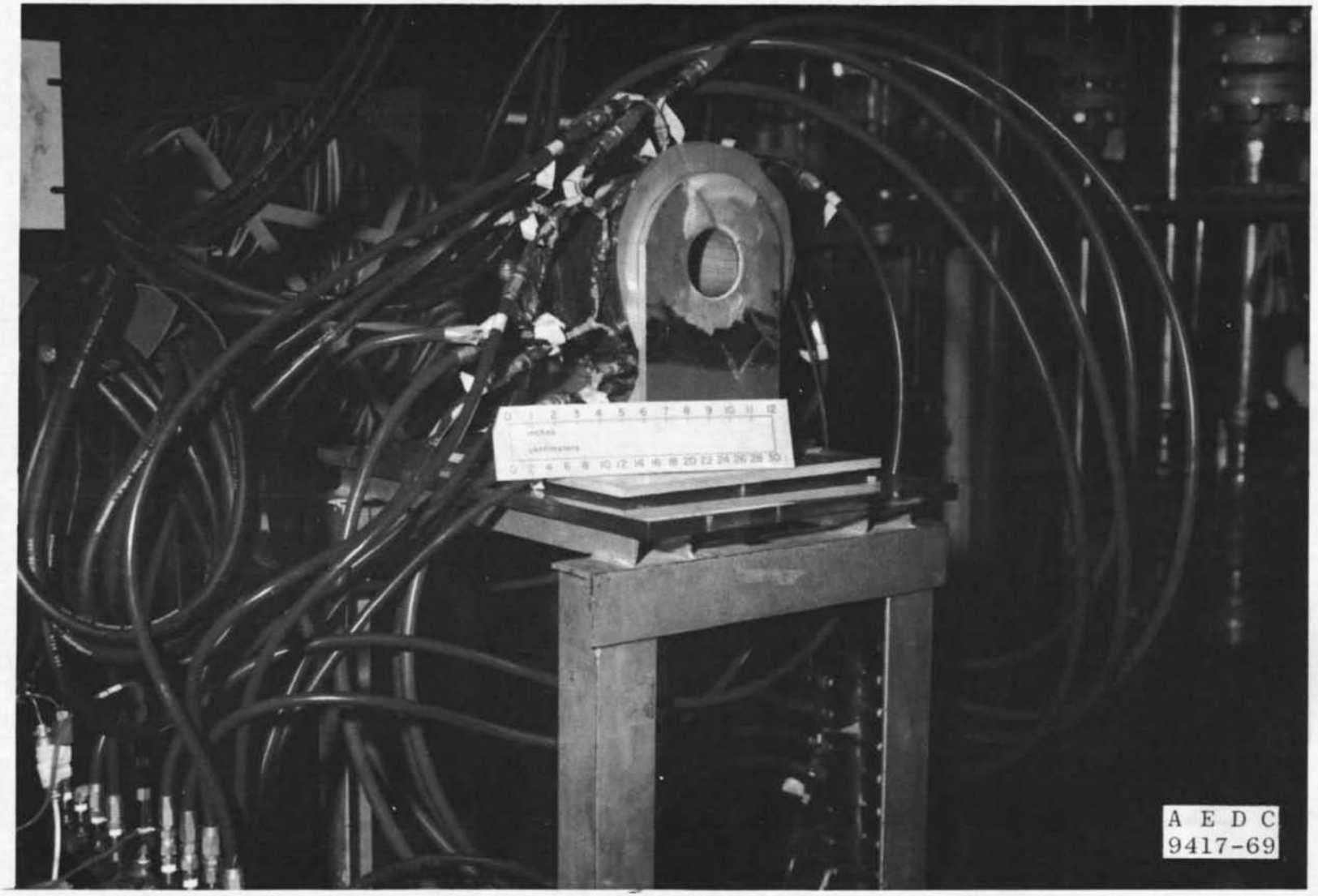

Fig. 5 Photograph of the 2.5-tesla Magnet

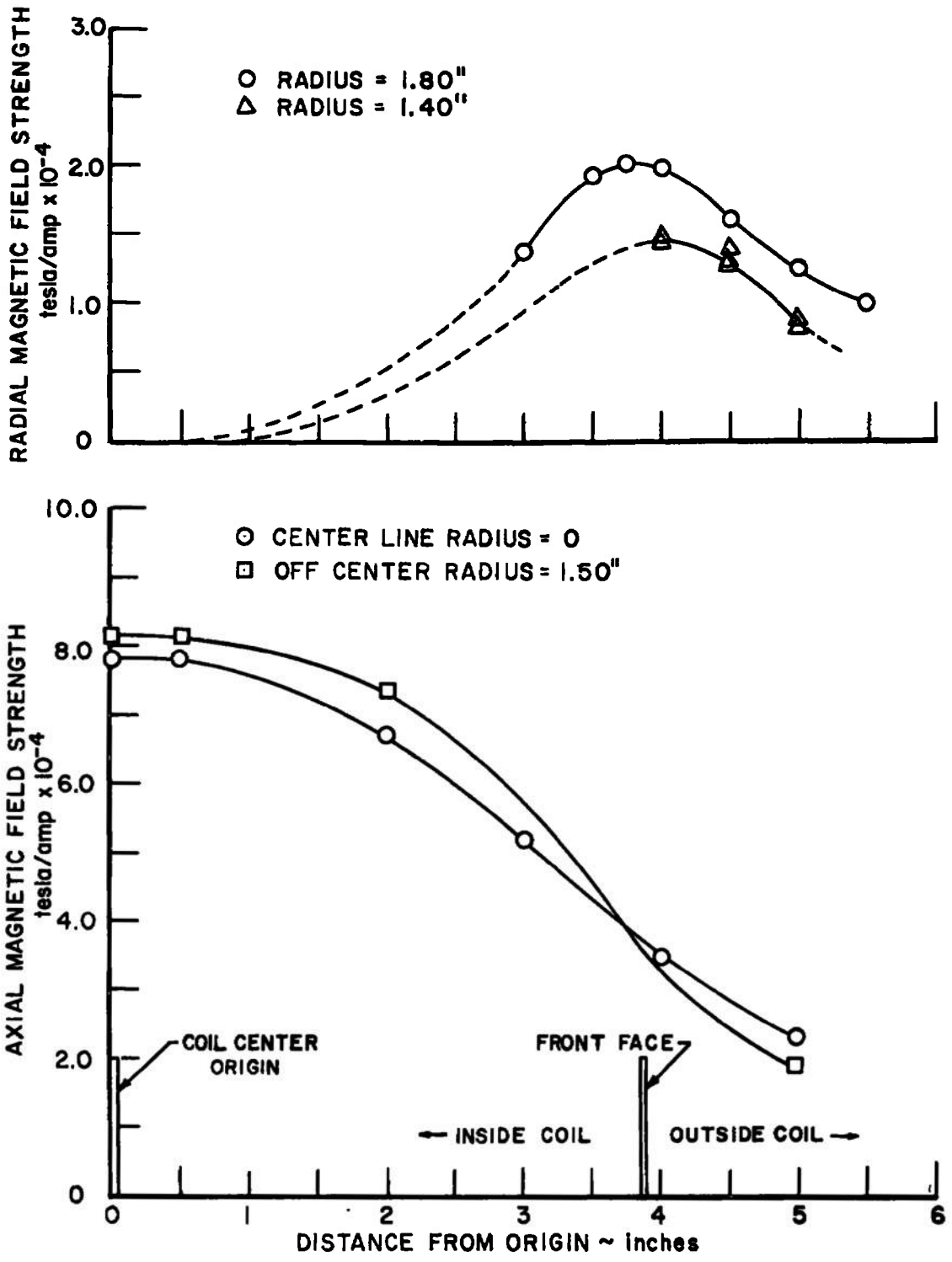

Fig. 6 Measured Magnetic Field Distribution of the 2.5-tesla Magnet

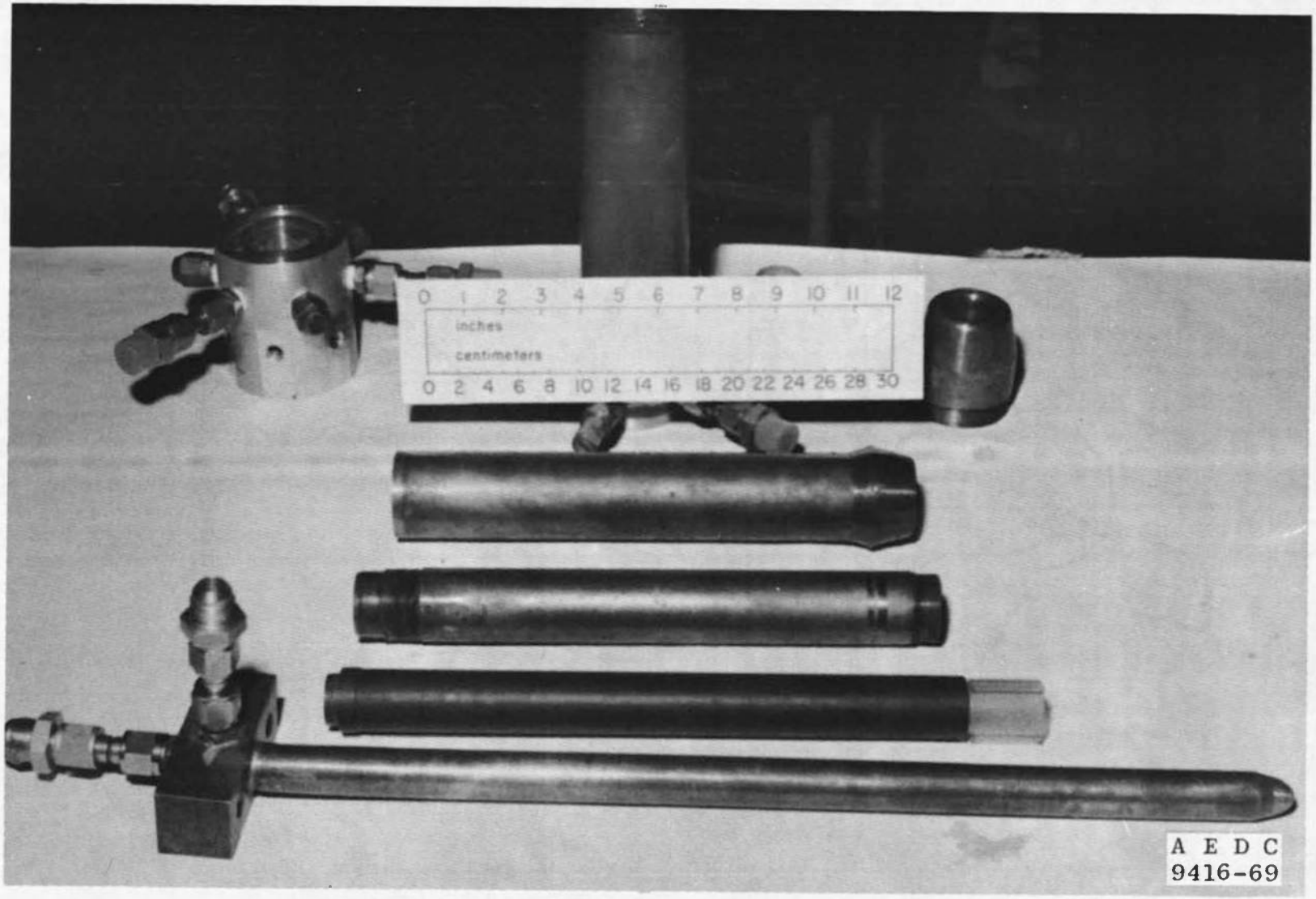

Fig. 7 Photograph of the Disassembled HP-2M

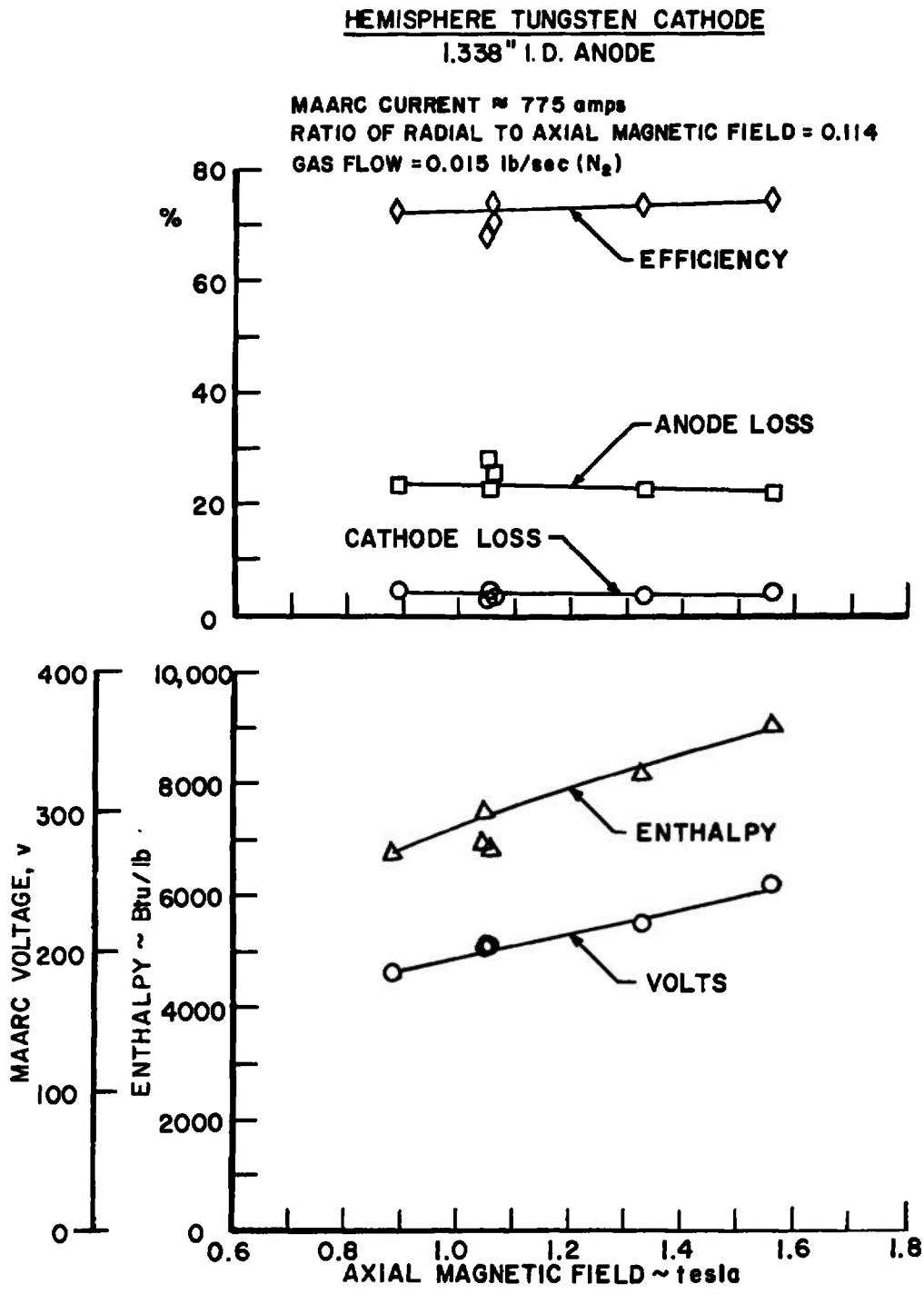

a. Tungsten Cathode

Fig. 8 Experimental HP-2M Data Showing the Effect of Changing the Axial Magnetic Field

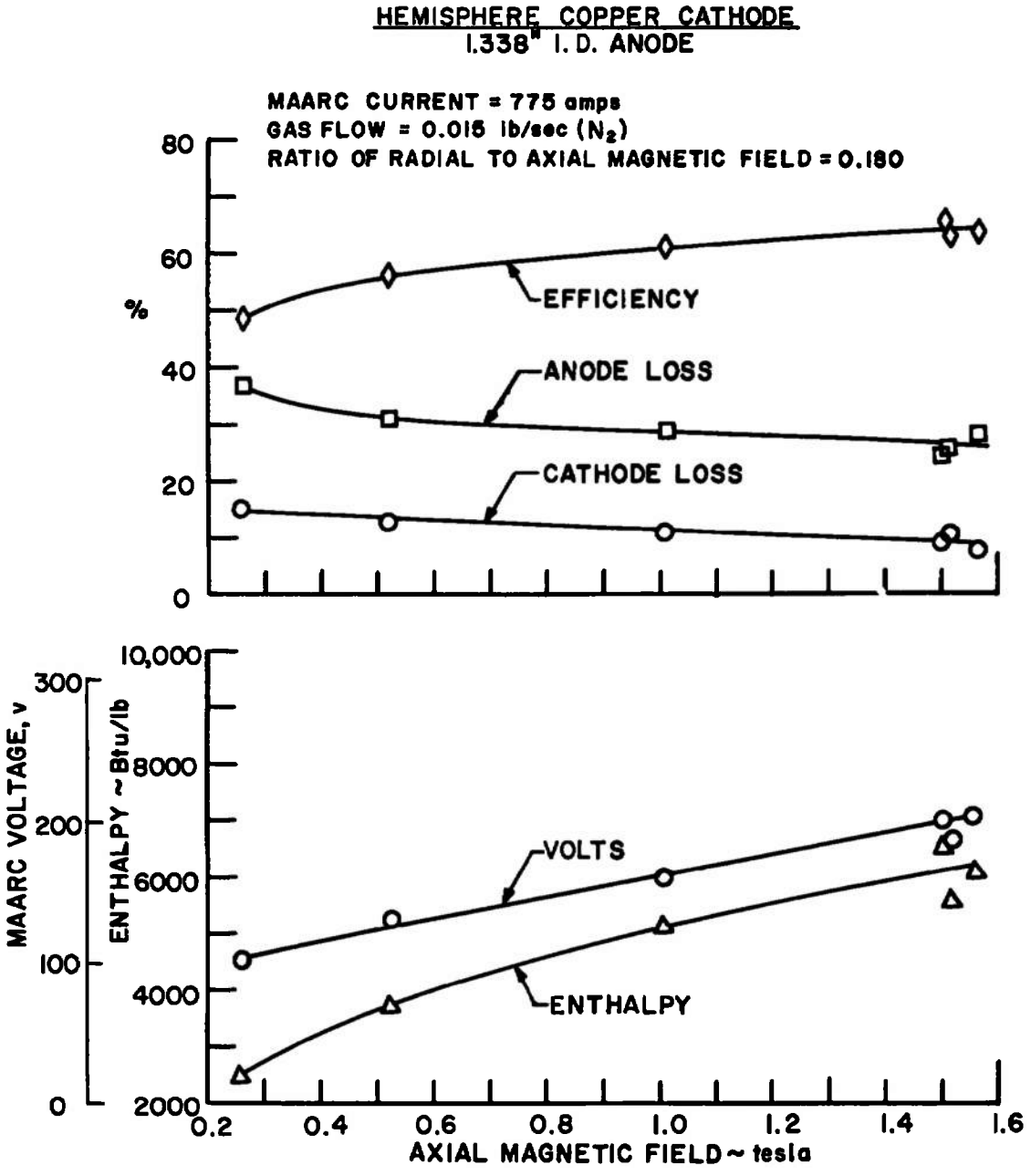

b. Copper Cathode
Fig. 8 Concluded

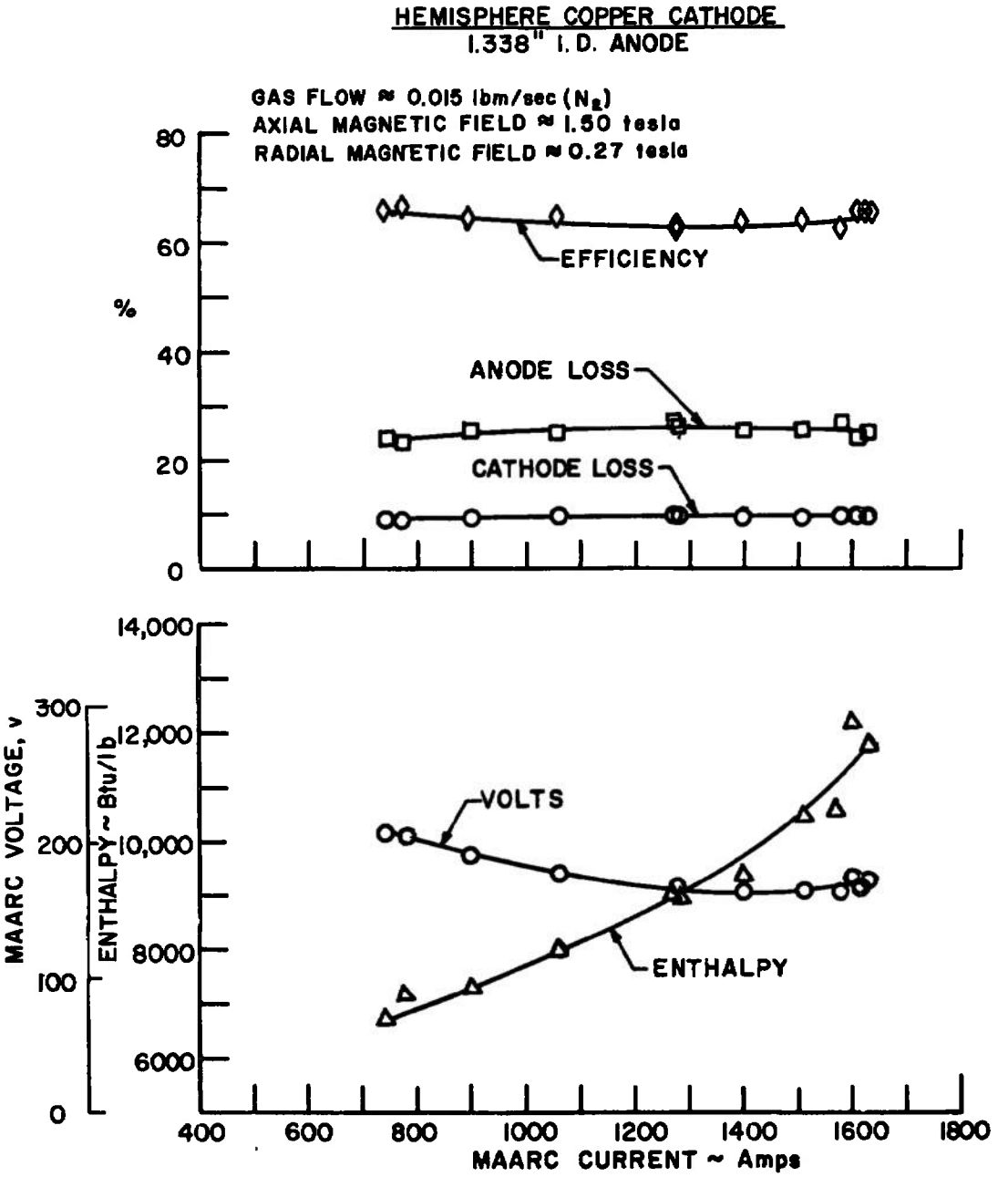

a. Axial Magnetic Field of 1.5 tesla

Fig. 9 Experimental HP-2M Data Showing the Effect of Changing the Current

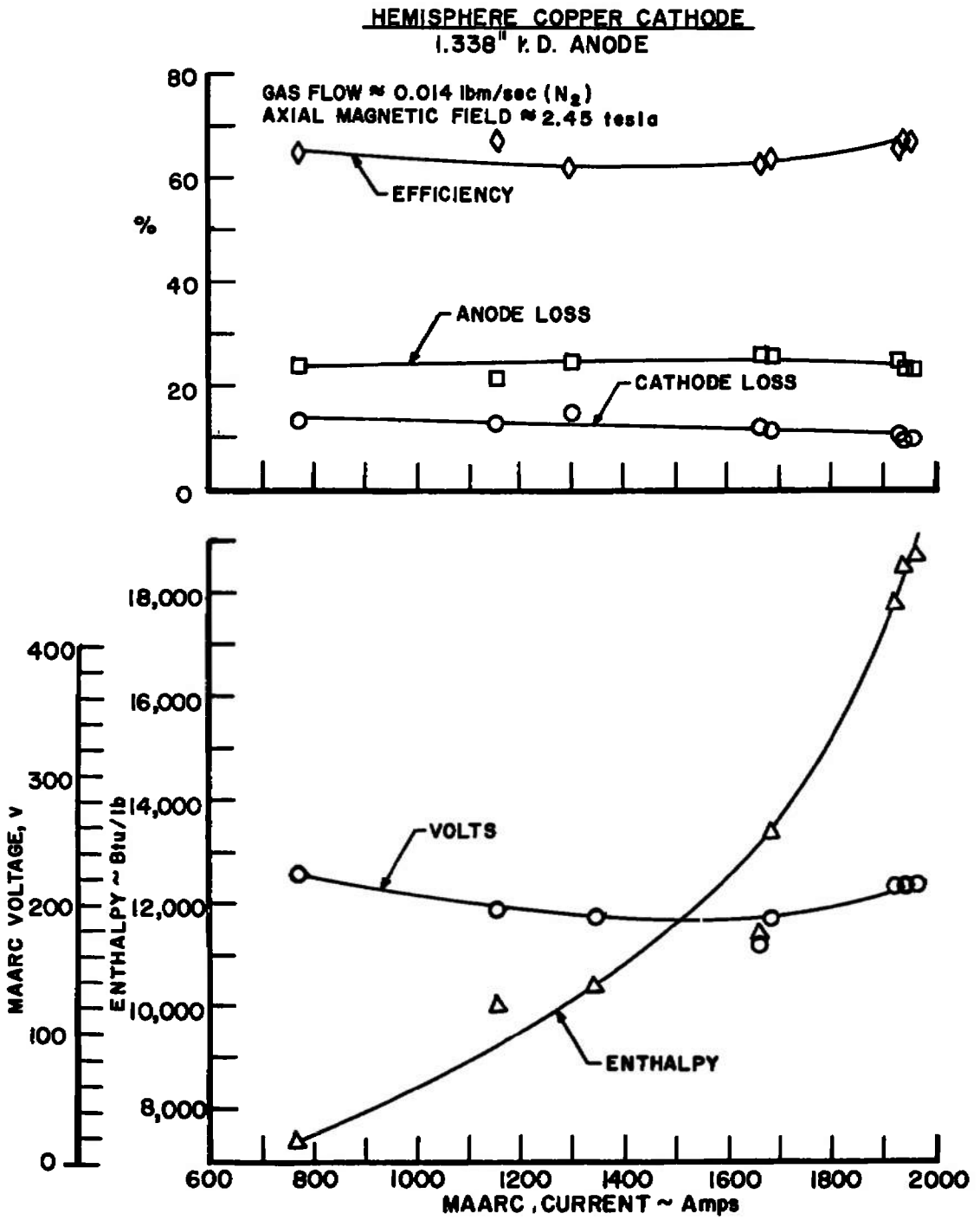

b. Axial Magnetic Field of 2.45 tesla
Fig. 9 Concluded

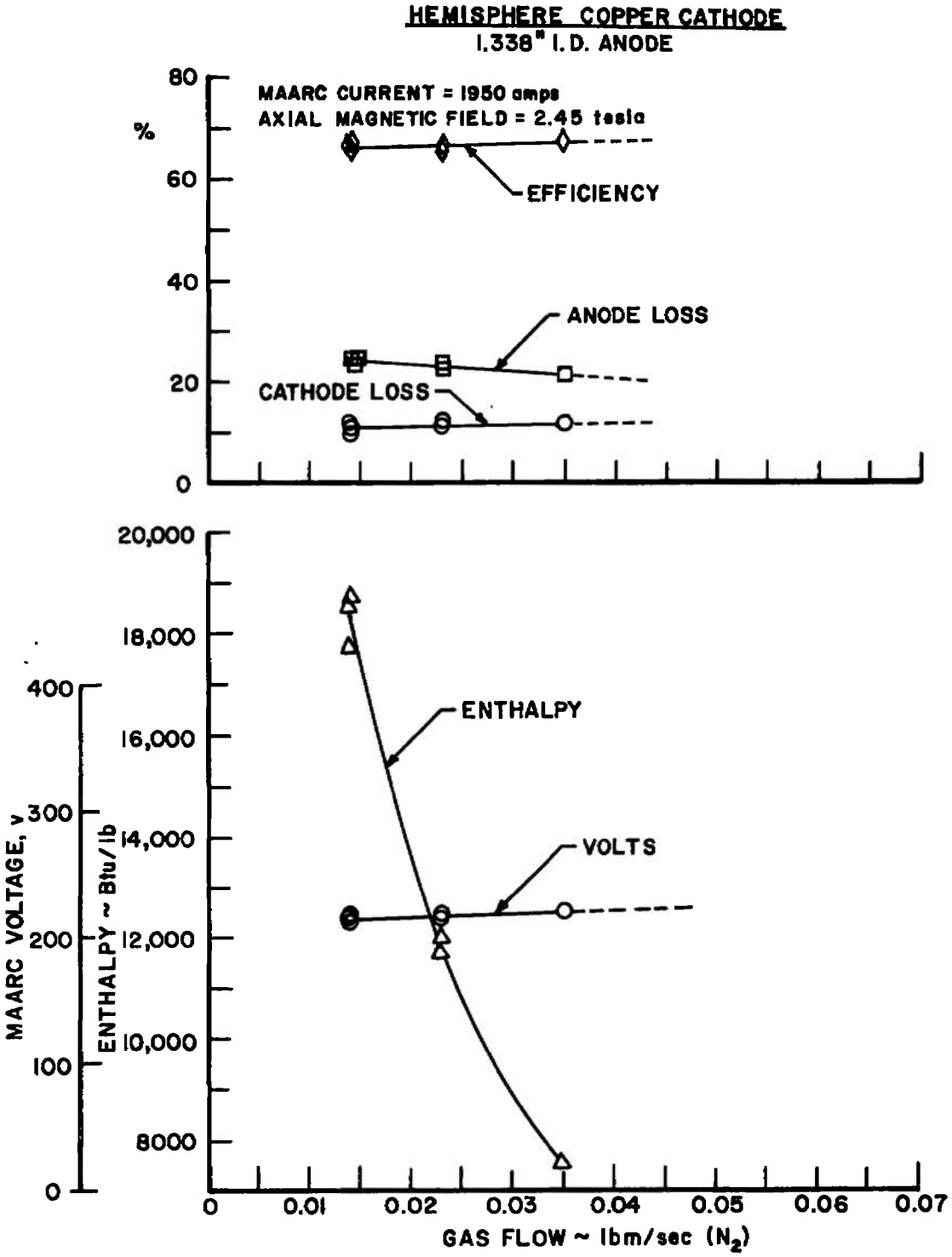

a. Axial Magnetic Field of 2.45 tesla and Current of 1950 amps

Fig. 10 Experimental HP-2M Data Showing the Effect of Changing the Gas Flow Rate

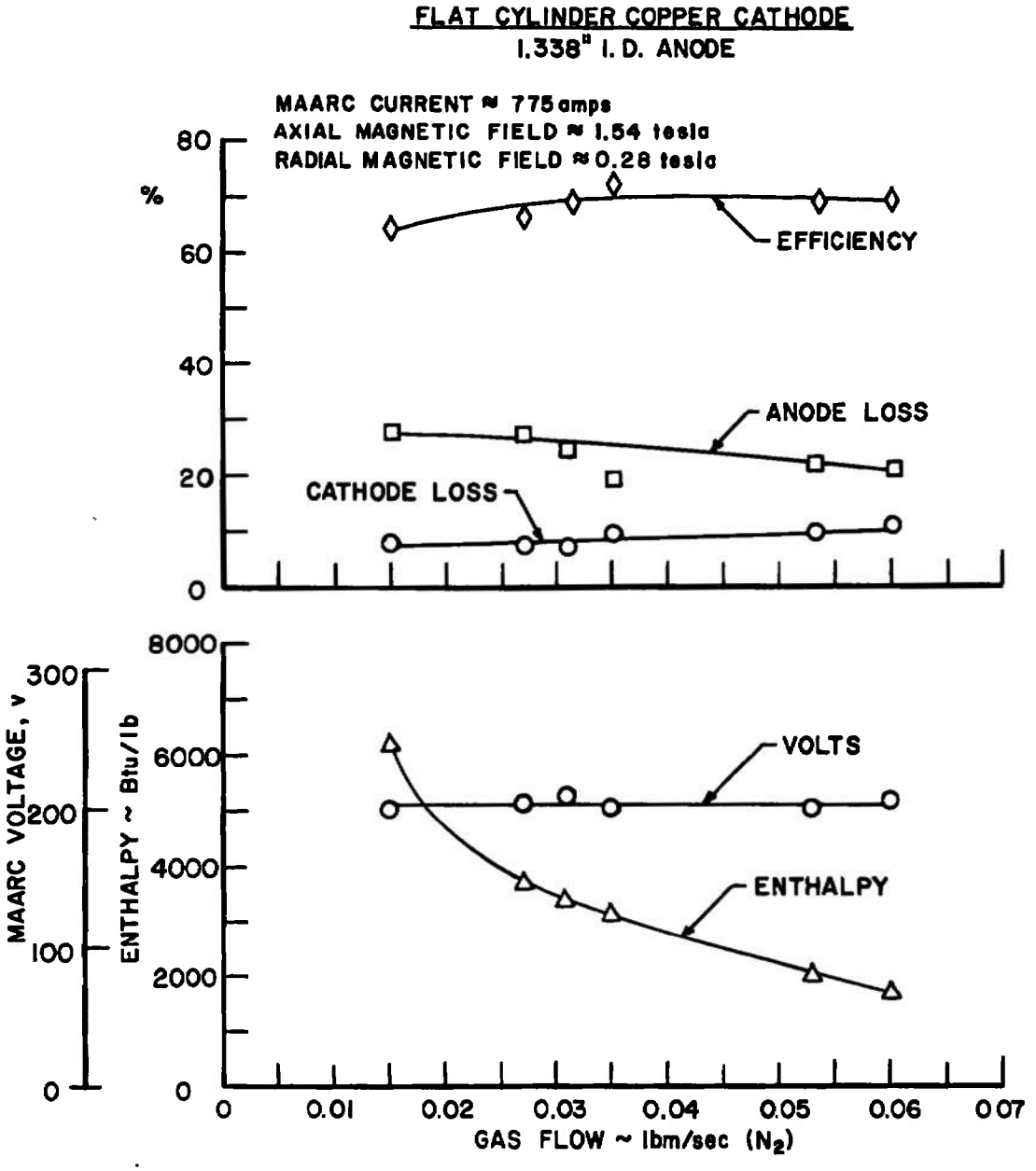

b. Axial Magnetic Field of 1.54 tesla and Current of 775 amps

Fig. 10 Continued

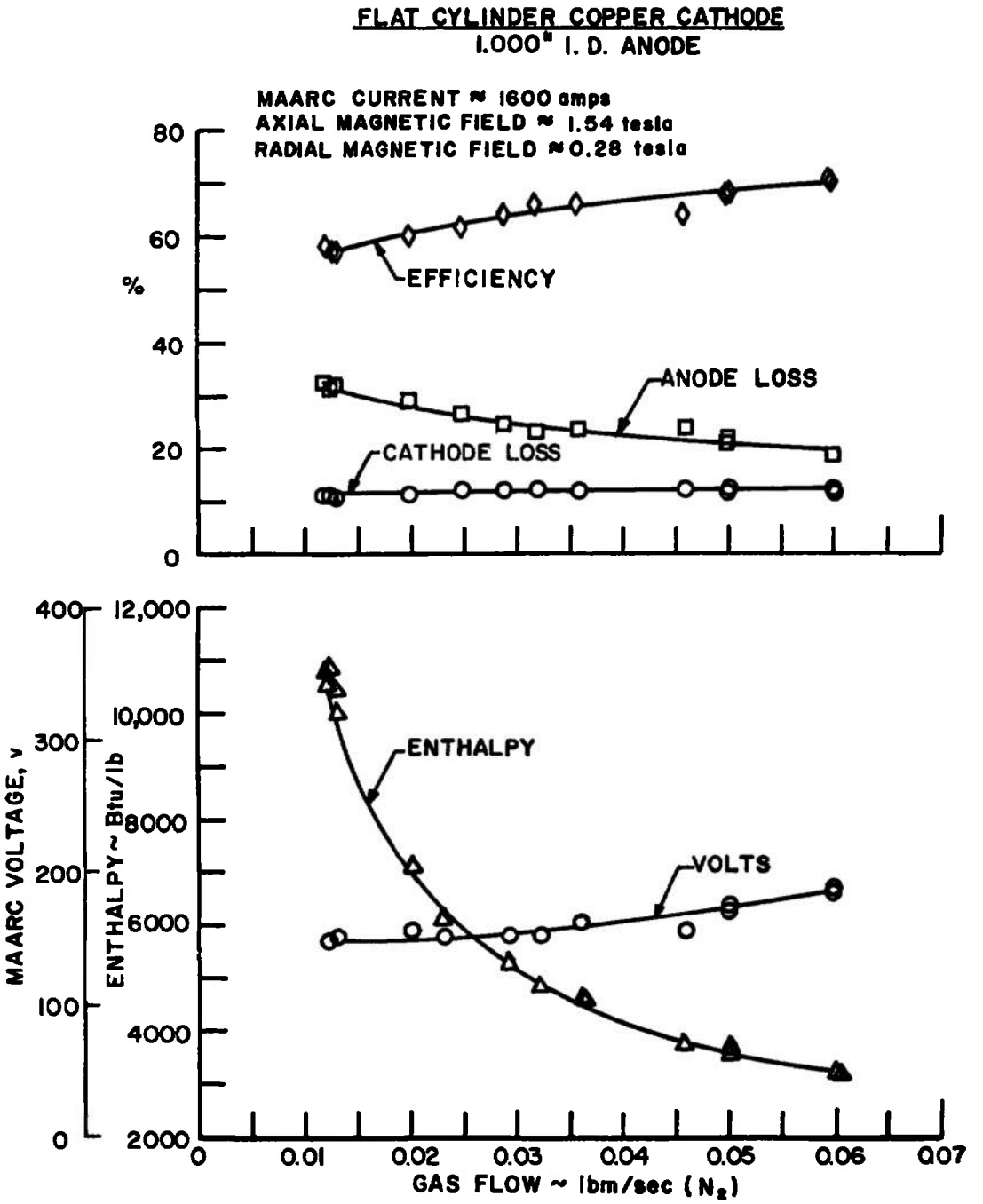

c. Axial Magnetic Field of 1.54 tesla and Current of 1600 amps Using a 1-in. ID Anode

Fig. 10 Continued

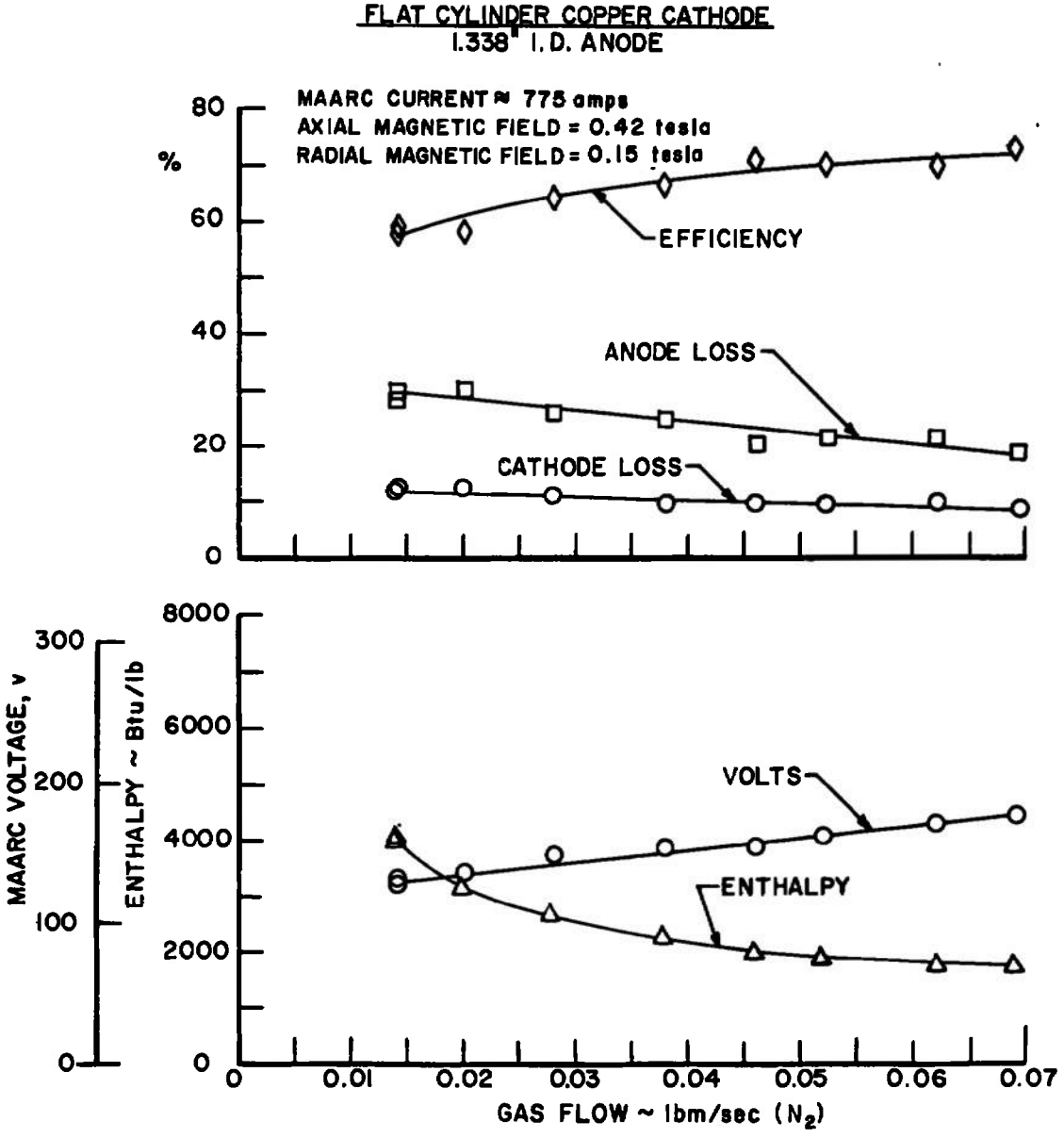

d. Axial Magnetic Field of 0.42 tesla and Current of 775 amps
Fig. 10 Continued

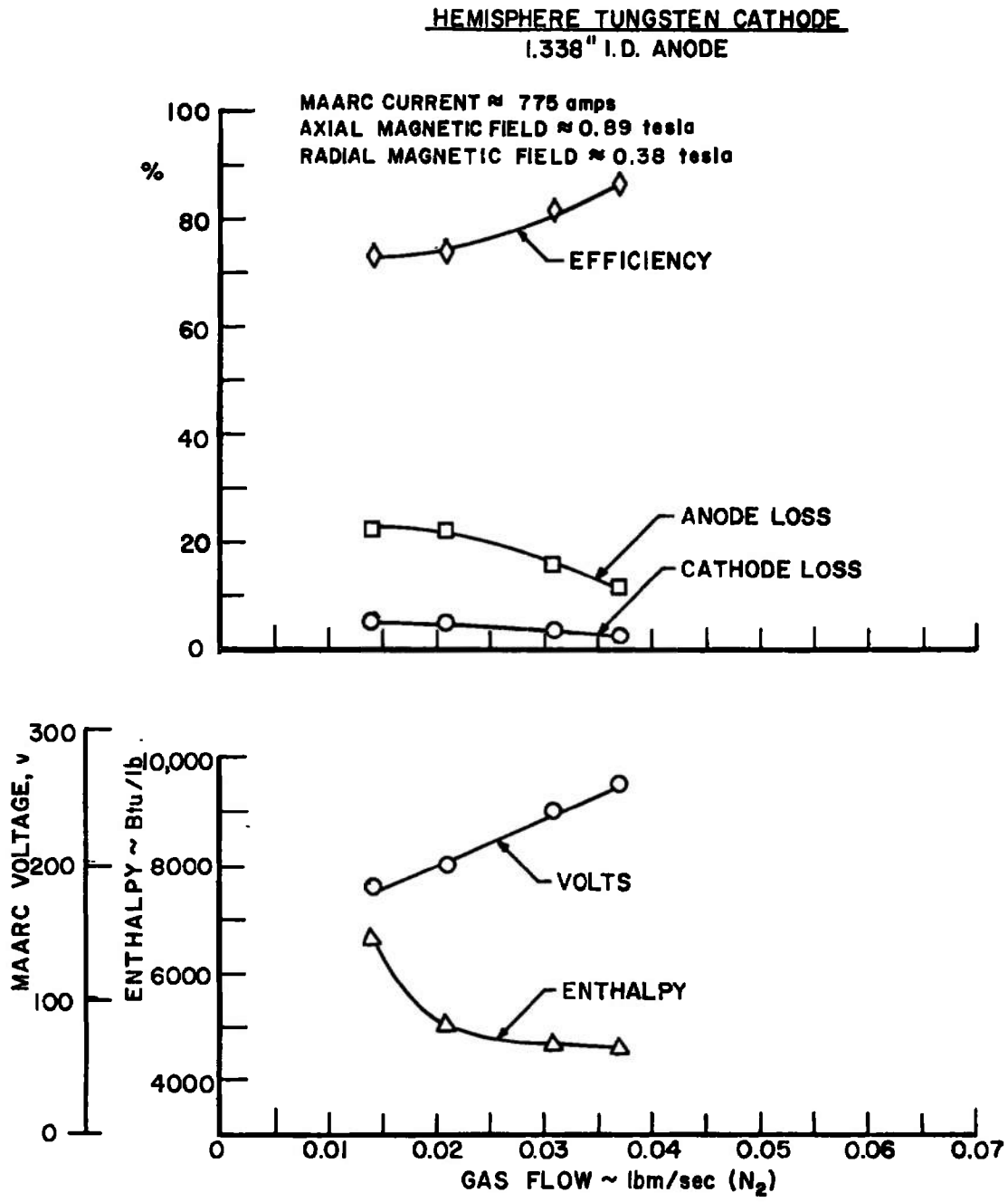

e. Axial Magnetic Field of 0.89 tesla and Current of 775 amps Using a Tungsten Cathode

Fig. 10 Concluded

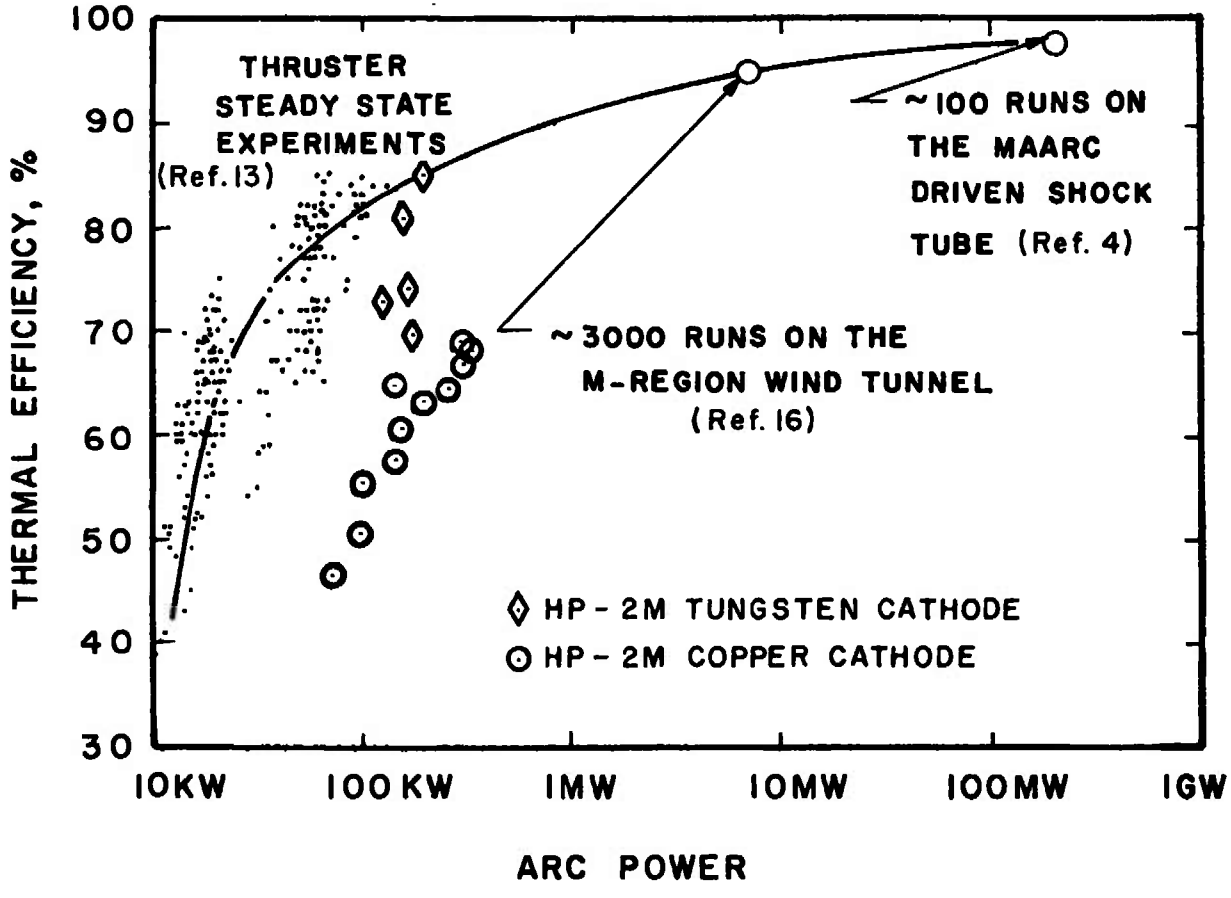

Fig. 11 Comparison of Thermal Efficiency of the AEDC Steady-State Atmospheric MAARC with the Data from the Low Pressure and Pulsed Experiments

Axial Field = 0.265 tesla, MAARC Current = 760 amps

a. Spoke Discharge

Axial Field = 1.514 tesla, MAARC Current = 745 amps

b. Transition Discharge

Axial Field = 1.529 tesla, MAARC Current = 1577 amps

c. Diffuse Discharge

Fig. 12 Consecutive High-Speed Photographs of the MAARC Discharge between the Center Cathode and Coaxial Anode (Frame Rate ≈ 10,000 frames/sec, Shutter Speed ≈ 2 μsec, Copper Electrodes)

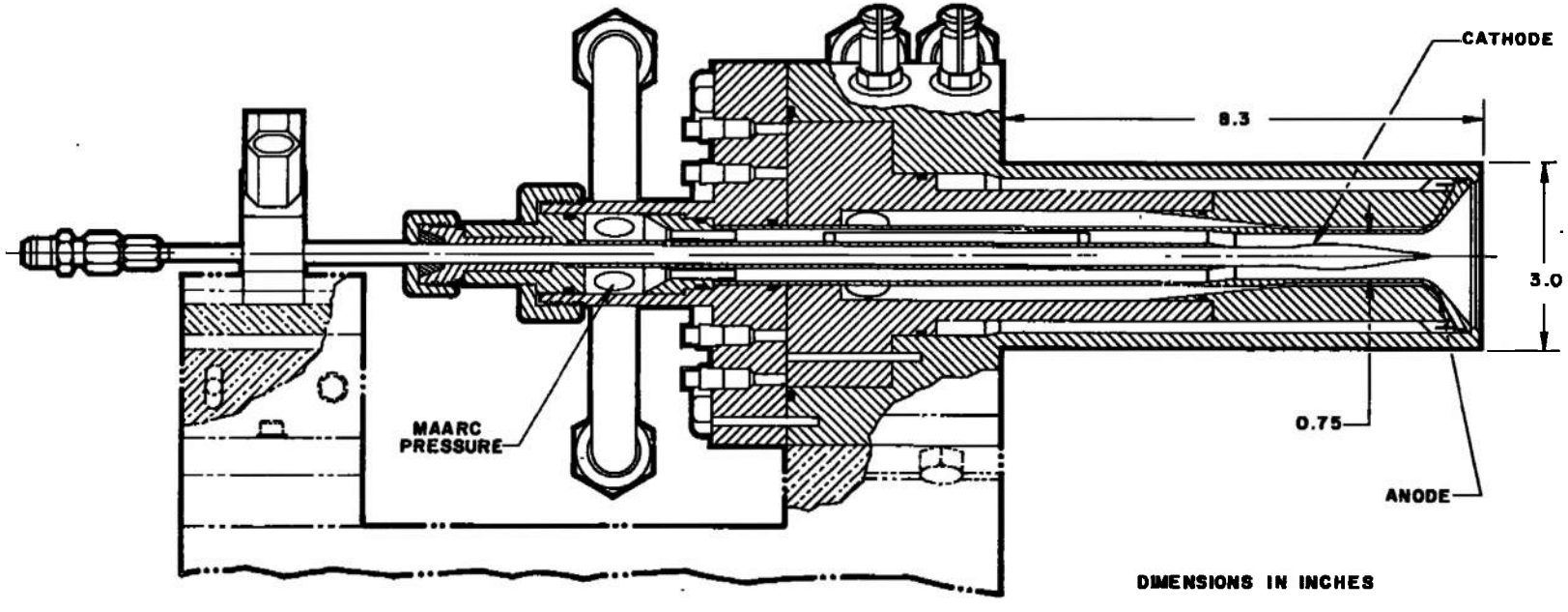

Fig. 13 Schematic of the Hera MAARC

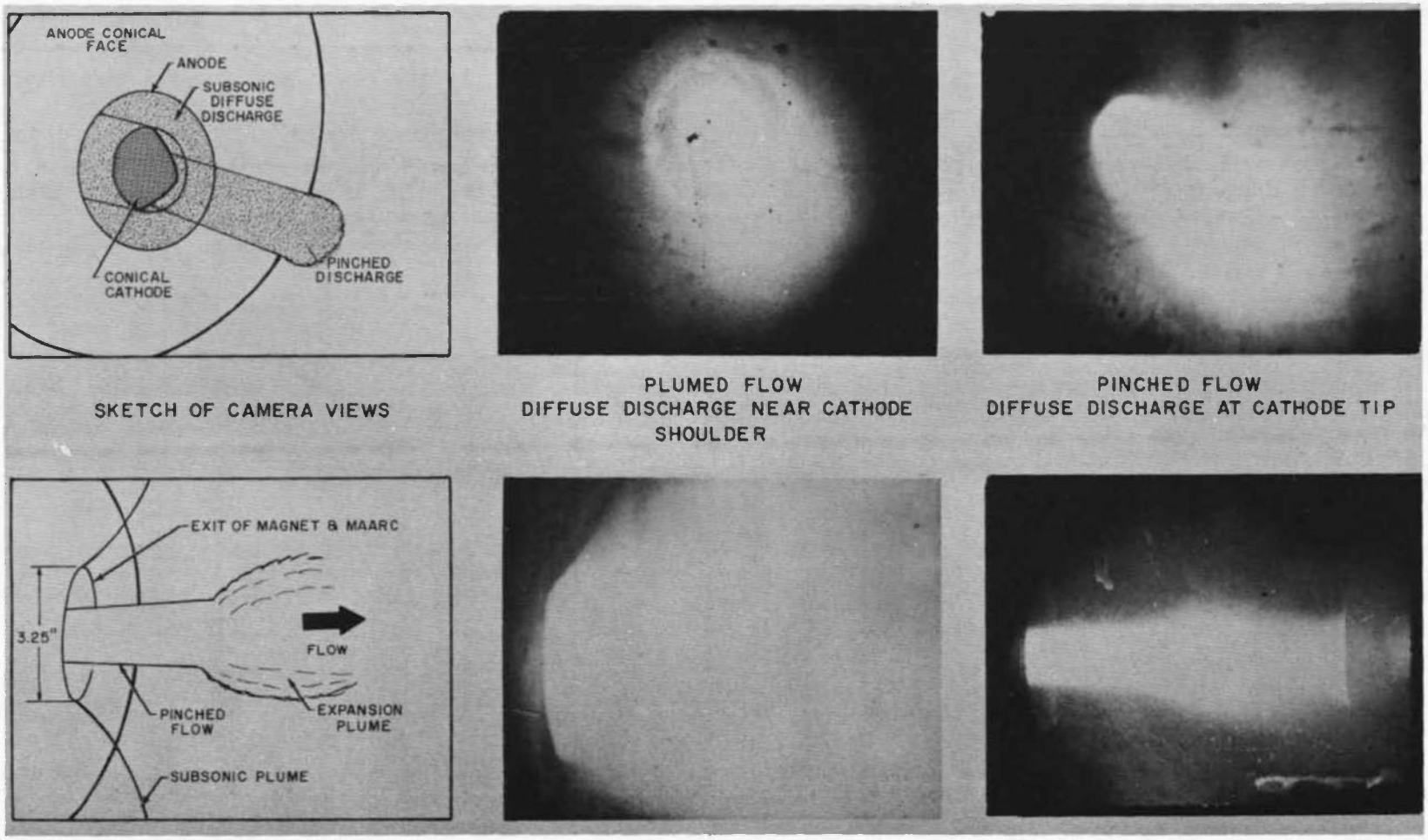

Fig. 14 Typical Flow Photographs Showing Both Operating Modes

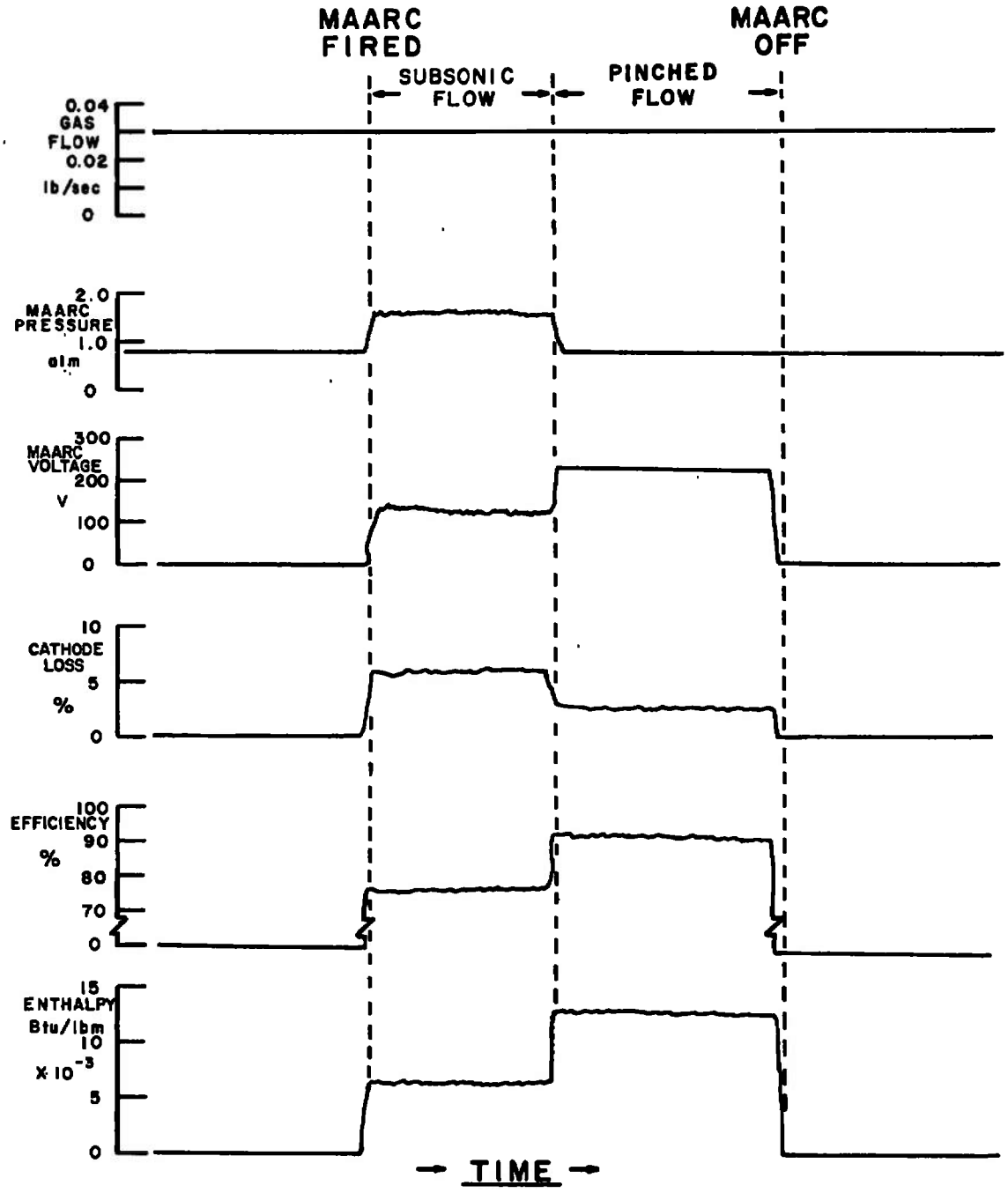

Fig. 15 Graphical Representation of the Hera MAARC Parameters Variation with Time

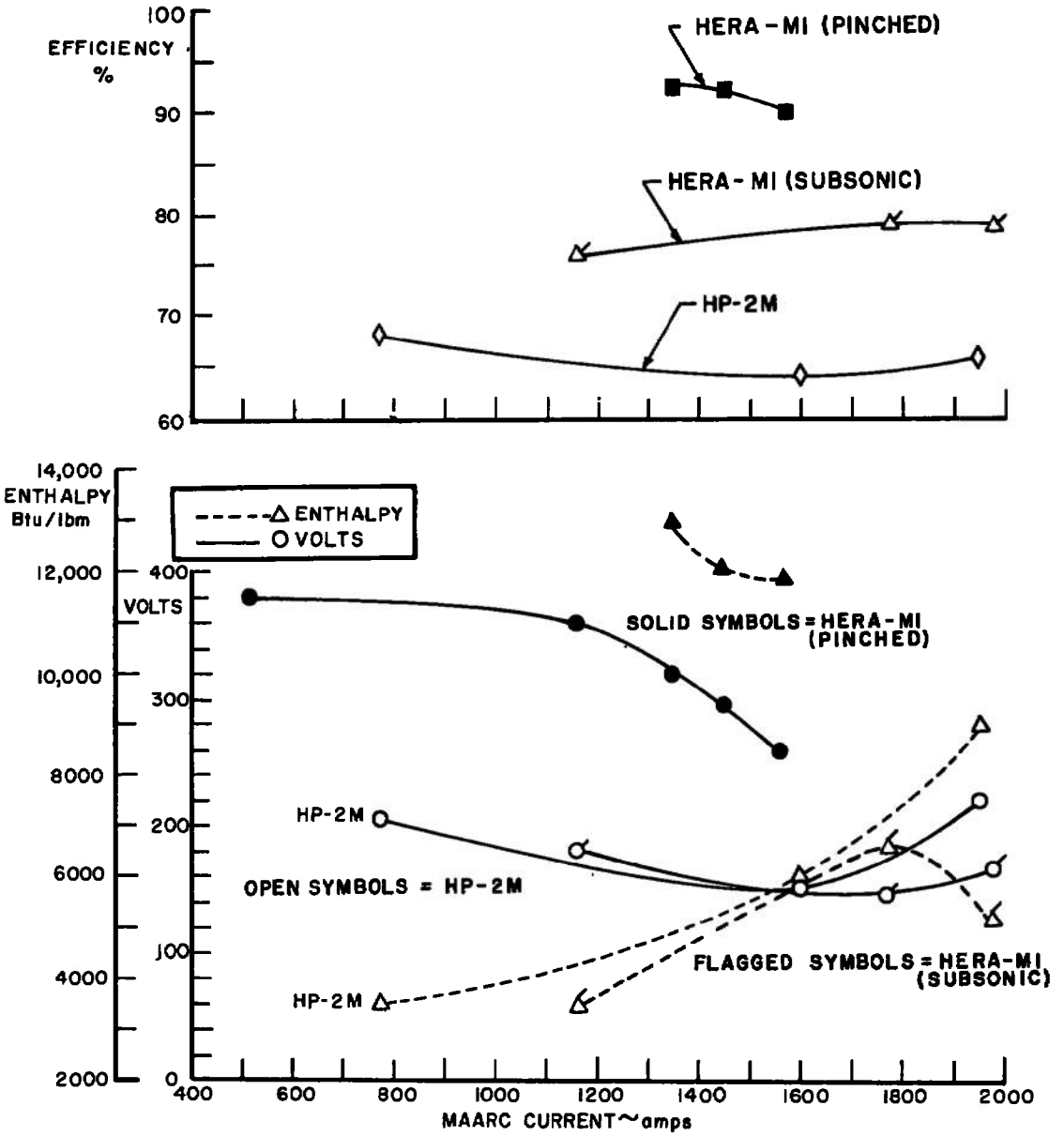

Fig. 16 Comparison of the Hera and HP-2M Operating Parameters with Increasing Current

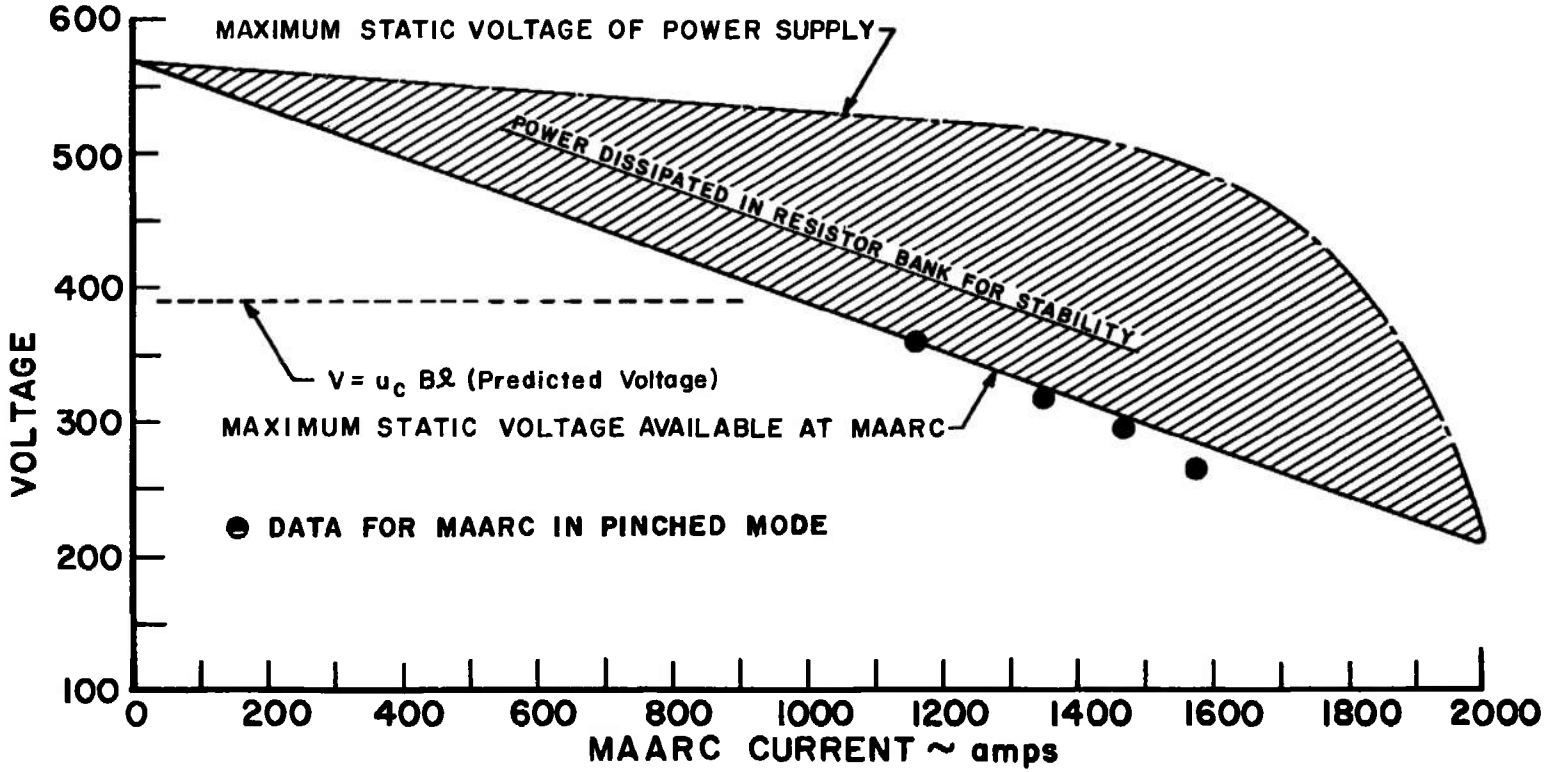

Fig. 17 Power Supply Limit of Hera MAARC Voltage

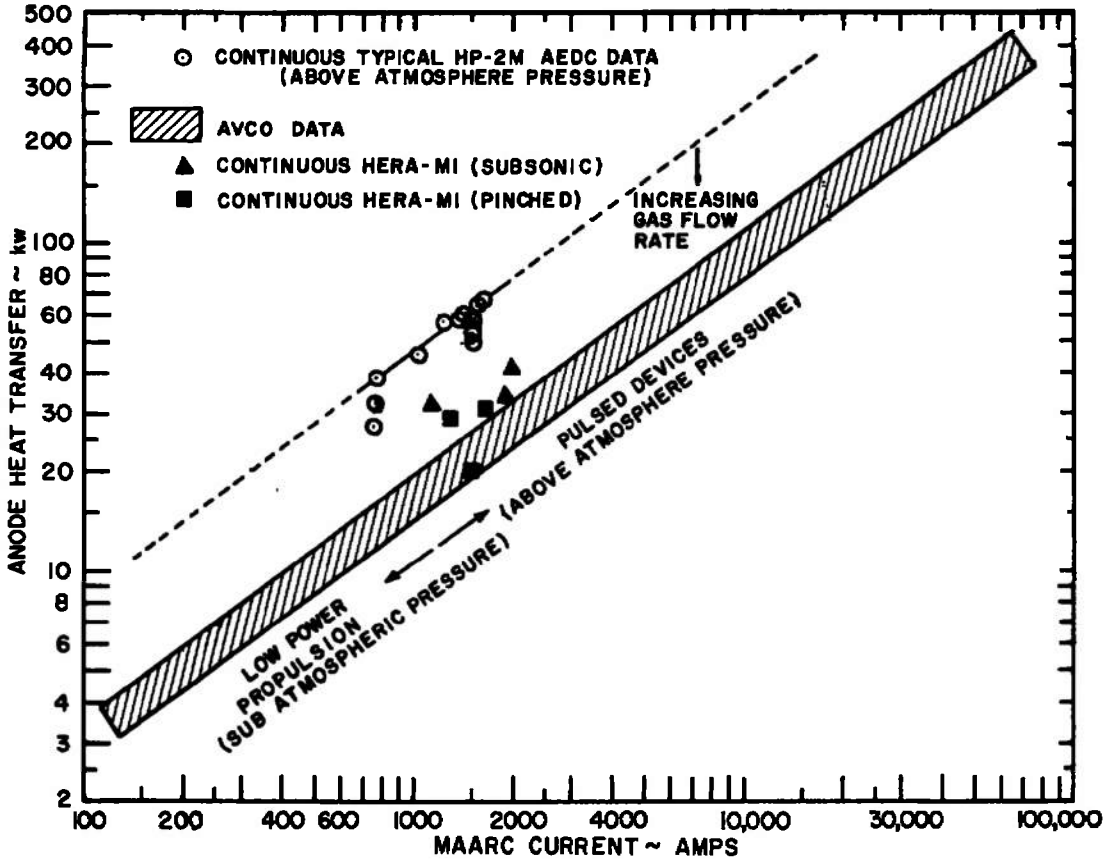

Fig. 18 Comparison of Anode Heat Transfer Data of Several MAARC Devices

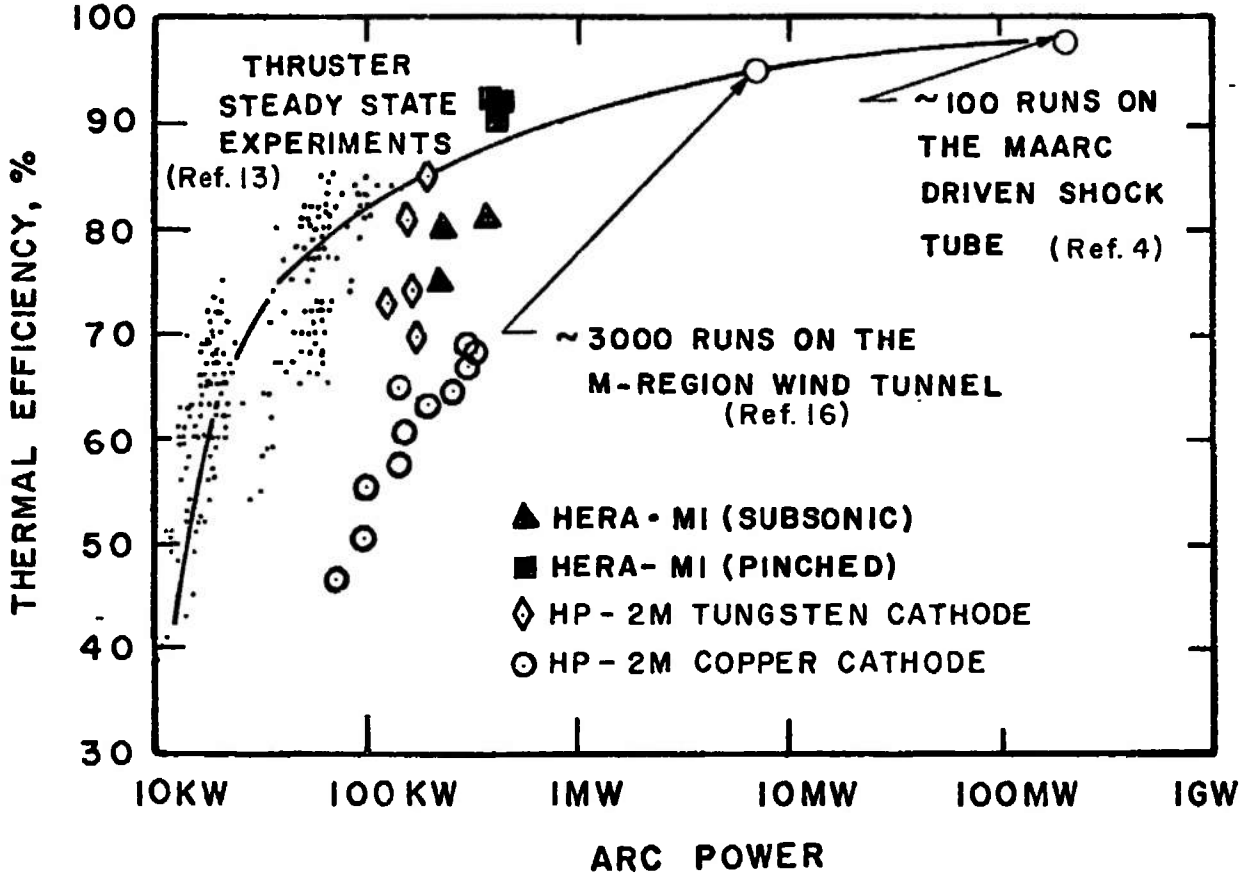

Fig. 19 Comparison of the Efficiency of Several MAARC Devices

TABLE I
TYPICAL MEASUREMENTS AND CALCULATIONS OF
HERA M1 OPERATING PARAMETERS IN NITROGEN

PARAMETER	SUBSONIC	PINCHED
V - volts	146	260
I - amp	1773	1570
P_g - MW	.259	.408
B - tesla	2.6	2.7
L_{CAT} - percent	7.4	2.7
L_{ANODE} - percent	11.2	5.4
$\dot{m}_{gas}$ - lbm/sec	.029	.029
H_o - Btu/lb	6927	12305
η - percent	81.4	91.9
p_o' - atm	.560	.337
$*p_o$ - atm	.100	1.430
p_o'/p_o	.179	4.250
d_{flow} - in/cm	Plumed	1.20/3.05

*Inferred through combining the measured flow rate and flow diameter with the assumption that all thermal energy is converted to kinetic energy. A factor of four increase in the stagnation pressure has been measured by Avco (Ref. 25).

TABLE II
PROJECTED PERFORMANCE OF MAARC FACILITIES

TYPICAL ARC HEATER	H_o Btu/lbm	p_o atm	p_o' atm (M = 1.7)	de in.	$H_o\sqrt{p_o'}$ $\times 10^{-3}$	$H\sqrt{p_o'}\ d_e^2$ $\times 10^{-3}$
5MW High Voltage	4,500 2,100	35 200	29.7 170.0	0.50 0.50	24.5 27.3	6.1 6.8
5MW Constricted	8,000 3,300	10 80	8.5 68.0	0.50 0.50	23.4 27.2	5.8 6.8
50MW High Voltage	2,800 2,500	20 122	17.4 104.0	1.20 1.10	11.7 21.5	16.9 31.0
(a) 1MW MAARC (Data)	12,500 (.4MW)	0.30	1.4	1.20	14.8	21.3
(a) 3MW MAARC (Projected)	70,000 7,000	2.3 7.5	10.1 32.0	0.75 0.75	223 39	125.0 21.9
(b) 16MW MAARC (Projected)	70,000 7,000	4.7 14.1	20.0 60.0	1.30 1.30	313 54	528.0 91.0
(b) 50MW MAARC (Projected)	70,000 7,000	11.8 35.3	50.0 150.0	1.30 1.30	495 86	835.0 145.0
125MW MAARC (Projected)	70,000 7,000	19.3 54.2	82.0 230.0	2.00 2.00	634 106	2535.0 426.0
Pulsed 200MW MAARC Shock Tube (Helium Data)	80,000	60	160.0 M > 3.0	1.50	1000	2250.0

(a)(b) Same devices operating with higher magnetic fields

APPENDIX III
EFFECT OF B-FIELD ON ABLATION TESTING

A large magnetic field is present in the MAARC and raises the question as to whether the magnetic field can significantly change the ablation characteristics of a model tested using the MAARC.

The possible effect of the magnetic field is investigated by comparing the $\vec{J} \times \vec{B}$ force and the inertia force $\rho u \frac{du}{dx}$ in the flow at some point on the body. B and u_∞ are assumed essentially parallel over the body cross section as shown in the following sketch:

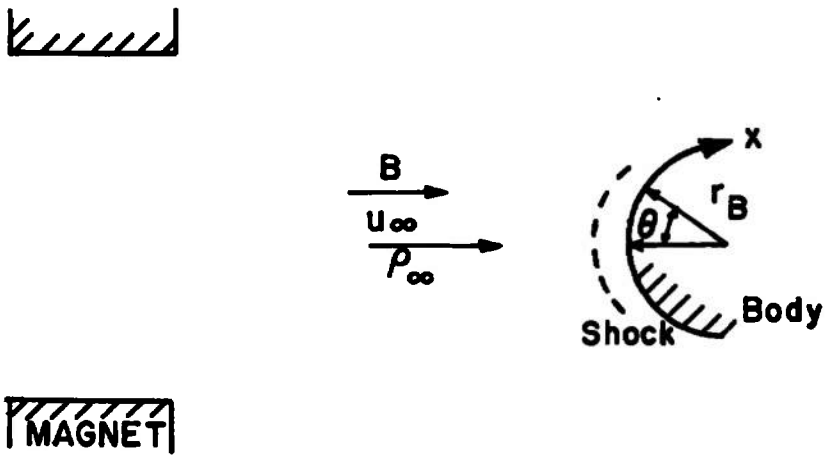

By using Newtonian theory, the pressure over the nose of the body is given by

$$p = p_o' \cos^2 \theta \tag{III-1}$$

and the velocity along the surface of the body is

$$u_B = \sqrt{\frac{2p_o'}{\rho_o'}} \sin \theta \tag{III-2}$$

The body force which will retard the flow is

$$|\vec{J} \times \vec{B}|_x = \sigma u_B B^2 \cos^2 \theta$$

so that an interaction parameter, S, is obtained:

$$S = \frac{|\vec{J} \times \vec{B}|_x}{\rho u \frac{du}{dx}} = \frac{\sigma B^2 r_B}{p_o'} \sqrt{\frac{ZRT_o'}{2}} \cos \theta \tag{III-3}$$

where r_B is the nose radius. This is seen to be a maximum at the stagnation point where $\theta = 0$ and σ is that corresponding to T_o'.

An evaluation of S for a rather severe operating point gives

$p_o' = 150$ atm
$H_o = 11{,}500$ Btu/lb
$r_B = 2.7$ cm
$B = 6.25$ tesla at the model

The magnetic field at the model has been taken to be one-fourth of the maximum value of the coil. The temperature is found from gas tables for air, $T_o' = 9400°K$. σ is computed to be 560 mho/m which gives $S = 0.058$ which indicates little interaction. This can be compared with the calculations of shock standoff distance by Porter and Cambel (Ref. 26) which show no change for $S < 1$.

One can ask whether the electrical conductivity could be greater in the boundary layer because of carbon ablation products. The ionization potentials,

N_2 - 15.51 ev	NO - 9.5 ev
N - 14.48 ev	CO - 14.1 ev
O - 13.55 ev	CO_2 - 14.4 ev

show that most of the electrons come from the NO and that the carbon products will reduce the conductivity.

It thus appears that the ablation rates will not be significantly affected by the large magnetic field associated with MAARC operation. This conclusion also holds for smaller scale MAARC since it can be shown for a given enthalpy H that S is independent of power in the gas.

UNCLASSIFIED

Security Classification

DOCUMENT CONTROL DATA - R & D

(Security classification of title, body of abstract and indexing annotation must be entered when the overall report is classified)

1. ORIGINATING ACTIVITY (Corporate author)	2a. REPORT SECURITY CLASSIFICATION
Arnold Engineering Development Center, ARO, Inc., Operating Contractor, Arnold Air Force Station, Tennessee 37389	UNCLASSIFIED
	2b. GROUP N/A

3. REPORT TITLE

DEVELOPMENT OF A MAGNETIC ANNULAR ARC OPERATING NEAR ATMOSPHERIC PRESSURE

4. DESCRIPTIVE NOTES (Type of report and inclusive dates)

July 1, 1969 to June 30, 1970 - Final Report

5. AUTHOR(S) (First name, middle initial, last name)

G. W. Garrison, Jr. and R. T. Smith, ARO, Inc.

6. REPORT DATE	7a. TOTAL NO. OF PAGES	7b. NO. OF REFS
November 1970	58	26

8a. CONTRACT OR GRANT NO.	9a. ORIGINATOR'S REPORT NUMBER(S)
F40600-71-C-0002	
b. Program Element 64719F	AEDC-TR-70-234
c. Facility Technology	9b. OTHER REPORT NO(S) (Any other numbers that may be assigned this report)
d.	ARO-PWT-TR-70-248

10. DISTRIBUTION STATEMENT This document is subject to special export controls and each transmittal to foreign governments or foreign nationals may be made only with prior approval of Arnold Engineering Development Center (XON), Arnold Air Force Station, Tennessee 37389.

11. SUPPLEMENTARY NOTES	12. SPONSORING MILITARY ACTIVITY
Available in DDC.	Arnold Engineering Development Center (XON), Arnold Air Force Station, Tennessee 37389

13. ABSTRACT

Two steady-state, high-pressure magnetic annular arc (MAARC) devices are compared experimentally to determine the potential of a MAARC as an ablation facility heat source. Data are presented verifying theory of operation in two modes, one subsonic and the other apparently supersonic. A comparison is made of projected MAARC devices and currently operating conventional high-pressure arc heaters for use as heat sources for high-shear ablation facilities.

This document has been approved for public release and its distribution is unlimited. Per A.F. Letter dtd 12 Feb. 73 signed by William O. Cole.

DD FORM 1 NOV 65 1473

UNCLASSIFIED

Security Classification

14. KEY WORDS	LINK A		LINK B		LINK C	
	ROLE	WT	ROLE	WT	ROLE	WT
magnetohydrodynamic generators						
high-shear ablation facility						
arc heaters						
solenoids						
magnet coils						
magnetic fields						
reentry vehicles						
mathematical model						
plasma control						